Investigations on Leak Before Break analysis

A thesis submitted to The University of Manchester
for the degree of Master of Philosophy in the Faculty of Engineering and Physical Sciences

2010

Christophe Mansoulié

School of MACE

TABLE OF CONTENTS

Final word count: 18 242 words

Table of Figures

Acknowledgments

I am heartily thankful to my supervisor, Dr Keith Davey of the University of Manchester, whose guidance, follow-up, and support during the project helped me greatly to achieve this work, particularly from a theoretical point of view.

Also, I would like to show my gratitude to some members of the team developing Code_Aster at EDF, beginning with Patrick Massin, who discussed with me some aspects of numerical programming, Samuel Géniaut for his explanations on numerical fracture mechanics, and Sylvie Michelle-Ponnelle for the time spent helping me with the software Ecrevisse.

I would like to thank Dr Dominique Laurence for having made this project possible in collaboration between EDF and the University of Manchester.

Lastly, I offer my regards and blessings to all of those who supported me in any respect during the completion of the project.

Christophe Mansoulié

Abstract

The present thesis was written by Christophe Mansoulié at the University of Manchester in pursuance of the degree of Master of Philosophy. It presents "Investigations on Leak-Before-Break (LBB) analysis" performed within the program of the British safety insurance company Serco to assess more complex Leak-Before-Break cases. Proceedings of British defect assessment code R6 on LBB analysis are summarised, and then the main focus is made on the computation of crack opening areas (COA) and stress intensity factors (SIF) for cracks in pipes and pressure vessels. A general overview of these methods is presented, and a comparison between two codes is made with regard to the numerical computation of SIF. The influence of the thermo-mechanical coupling of the structure with the fluid is investigated using enhancements of numerical tools from the French company EDF, concluding to a possible significant change in flow rates found. From there general theoretical methods to analyse linear thermo-elastic fracture mechanics problem are considered, and in particular a simpler thermo-mechanical model of an infinite plate containing a crack subjected to uniform heat flux. An application of crack opening area calculation is made for this case, and difficulties of modelling in thermo-elastic fracture mechanics are raised. In the scope of Serco's program also including the assessment of complex geometries, a numerical investigation of one typical example of their effect on COA and SIF is performed in the case of continuous thickness transitions in pipes, for which a shielding effect is brought to light.

Declaration and copyright statement

The author of this thesis certifies that no portion of the work referred to in the thesis has been submitted in support of an application for another degree or qualification of this or any other university or other institute of learning.

i. The author of this thesis (including any appendices and/or schedules to this thesis) owns certain copyright or related rights in it (the "Copyright") and s/he has given The University of Manchester certain rights to use such Copyright, including for administrative purposes.

ii. Copies of this thesis, either in full or in extracts and whether in hard or electronic copy, may be made **only** in accordance with the Copyright, Designs and Patents Act 1988 (as amended) and regulations issued under it or, where appropriate, in accordance with licensing agreements which the University has from time to time. This page must form part of any such copies made.

iii. The ownership of certain Copyright, patents, designs, trade marks and other intellectual property (the "Intellectual Property") and any reproductions of copyright works in the thesis, for example graphs and tables ("Reproductions"), which may be described in this thesis, may not be owned by the author and may be owned by third parties. Such Intellectual Property and Reproductions cannot and must not be made available for use without the prior written permission of the owner(s) of the relevant Intellectual Property and/or Reproductions.

iv. Further information on the conditions under which disclosure, publication and commercialisation of this thesis, the Copyright and any Intellectual Property and/or Reproductions described in it may take place is available in the University IP Policy (see http://www.campus.manchester.ac.uk/medialibrary/policies/intellectual-property.pdf), in any relevant Thesis restriction declarations deposited in the University Library, The University Library's regulations (see http://www.manchester.ac.uk/library/aboutus/regulations) and in The University's policy on presentation of Theses

Nomenclature

Roman symbols

A	mean crack opening area
A_0	crack opening area for a flat plate
$A_{0/ex}$	crack opening area at entrance or exit
$\underline{\underline{\underline{A}}}$	elasticity tensor
C_D	discharge coefficient
d	divergence crack parameter
E	Young's Modulus
f	friction Fanning factor
F	friction loss factor
$F_{(t/b)}$	Folia's bulging factor (tension or bending)
G	energy release rate
h	Newton's coefficient of convection
j	heat flux
k	structure conduction coefficient
K	stress intensity factor in mode I (unless otherwise specified)
l	semi crack length
l_c	critical semi crack length
l_{eff}	effective crack length
l_t	length of thickness transition
L	idealised length for a rectangular crack
M	moment load
p, γ	densities of potential for temperature
$p_{0/ex}$	pressure at crack entrance or exit
P	force load
Q	flow rate
r	cylindrical coordinate from crack tip or heat source
r_E	smallest external radius
r_I	internal radius
r_p	plastic zone size
R	mean radius of a pipe
R_a	surface roughness coefficient
R_E	biggest external radius
s	curvilinear coordinate along crack path
t	shell thickness
T	temperature
$\underline{T}^d$	Imposed stresses
u	normal displacement on crack face or edge
$\underline{u}$	Displacement field
U_t	total deformation energy
v	fluid velocity at exit

$w_{0/ex}$ crack width at entrance or exit

W idealised rectangular crack width

x coordinate along crack axis

y coordinate normal to crack axis

Greek symbols

α thermal dilatation coefficient

$\alpha(\lambda)$ bulging factor for COA

δ maximum crack opening displacement

ε_{ref} reference strain

$\underline{\underline{\varepsilon}}$ strain field

η crack propagation parameter

θ crack angle

$\underline{\theta}$ virtual crack extension velocity

λ thin shell parameter

λ, μ Lamé's coefficient

ν Poisson's coefficient

ρ thin shell parameter for internal pressure

$\rho_{0/ex}$ density at crack entrance or exit

σ constant normal or remote tensile stress

σ_d imposed normal stress on crack edges

σ_{ref} reference stress

σ_Y yield stress

$1/\chi$ characteristic decay length of temperature

ψ strain energy field

1 Principles of Leak-Before-Break Analysis

1.1 Presentation of Leak Before Break Arguments

There are several options to demonstrate the safety of a structure containing defects when an initial assessment has failed to show that adequate margins exist or, inversely, to size a structure with less penalising requirements. For pressurised components, namely pipes and pressure vessels, one of these options is to make a Leak-Before-Break case. The purpose of a LBB argument is to demonstrate that leakage of fluid through a crack that has penetrated through the wall in a pressurised component can reach a stable detectable flow rate prior to the crack attaining a critical size at which catastrophic failure like a sudden disruptive break could occur.

Historically nuclear power plants have been designed to resist to the most severe reactor loss of coolant accident (LOCA) which is a postulated double ended guillotine break (DEGB) in high energy piping systems. Sizing pressure retaining parts for these events of very low probability even under severe accidental conditions resulted in the construction of massive pipe-whip restraints and jet impingement shields with an important economical impact. That is why the LBB concept has been developed as an alternative approach to avoid having to consider dynamic effects of these breaks. The history and specific methodologies up to 1993 are presented in [7] and a compound of all useful concepts and their application in different countries are described in [19].

The United States Nuclear Regulatory Commission (USNRC) and the German Reaktorsicherheitskommission (RSK) have been the first to perform extensive research and development on this subject and implemented legislative rules. In the case of the USA they would enable a design relieved of the dynamic effects of DEGB based on detectable leakage for idealised through-wall cracks (the Modification of General Design Criterion 4 (GDC-4) and the Standard Review Plan (SRP) 3.6.3 published in 1987 on LBB concept, together with Section XI of ASME Code). On the other hand, in Germany, the dynamic effects of leaks only (as opposed to breaks) and the crack propagation from a surface defect would be taken into account as an additional safety within the concept of Break Preclusion, originally used for the design of advanced Convoi plants and now for the design of EPR (Evolutionary Power Reactor) by Areva.

But actually Yonggwang 3 and 4 in South Korea are the first nuclear power plants in the world that adopted the LBB concept in early stages of design. In China, the Institute of Nuclear and New Energy Technology used it for the design of 10-MW HTGR. In Japan, it has

been implemented in a similar way as in Germany by the Japan Electric Association that published in 1999 the "Technical Guidelines for Protection Design Against Postulated piping Failures in Nuclear Power Plants," JEAG 4613-1998 for austenitic stainless steel piping only. In France, LBB has been applied to LMFBR and a guideline for LBB assessment is included in the flaw evaluation guide A16, for LMFBR developed by Commissariat à l'Energie Atomique (CEA), where guidelines are given for analysis of the growth up to a full through-wall crack. Also in the case of the French electricity company EDF, investigations are conducted for reinforced concrete studies. In the United Kingdom, the R6 procedure [14] developed in 2001 - R6 Panel composed of British Energy, Rolls-Royce, Serco and TWI - prescribes the two approaches, from the propagation of a surface defect, to the detectable leak through an idealised through-wall crack, and also unique rules for the effect of creep on LBB arguments - based on assessment of creep effect in R5. LBB has been applied to several steel components in order to strengthen safety justifications in the UK nuclear industry.

This section is a summary of LBB procedures in the British assessment of defects code R6.

1.2 Flaw characterization, estimation of defect length at breakthrough and of stability

- The defect length at breakthrough is the length that it takes when it becomes a through-wall crack just after unstable propagation through the thickness.
- The limiting defect length is the length at which disruptive failure is estimated to occur.

In order to assess real flaws, it is needed to model a known or postulated crack by choosing an adequate and conservative shape. In R6, guidance is provided as to which shape to take and rules are given about the calculation of the limiting defect length and the defect length at breakthrough [14].

Stress intensity factors (SIF) are important parameters as they are required to enable critical crack size (in other words limiting defect length) to be evaluated by way of defect assessment procedures like R6. In most cases it is conservative to consider only the most damaging stress intensity factor K_I in mode I. These stress intensity factors can be evaluated in Finite Element Analysis by means of the G-θ method (developed in section 3.4) which consists in using the bilinear form of the energy release rate G expressed as an integral of a virtual crack extension field θ. This method facilitates the calculation of G or the J-integral which is a path-independent field integral equal to G in linear elasticity, and all stress intensity factors (in linear elasticity only, where the different loading modes can be distinguished). Formulae are

readily available in literature for a vast number of simple configurations under basic loads such as pressure, membrane and bending loads.

1.3 Law of stable crack growth during a pressurised component's lifetime

In order to assess that during crack birth, growth and penetration and up to unstable expansion, sufficient fluid leakage will be released and enough time will be left after detection to take action before failure, it is necessary to evaluate precisely the different stages of the evolution of a crack. The British defect assessment procedure R6 [14] presents a synthesis of the experience gathered in the nuclear industry compounding a significant amount of theoretical, numerical, experimental and field observation data, and provides guidance about predicting crack assessment.

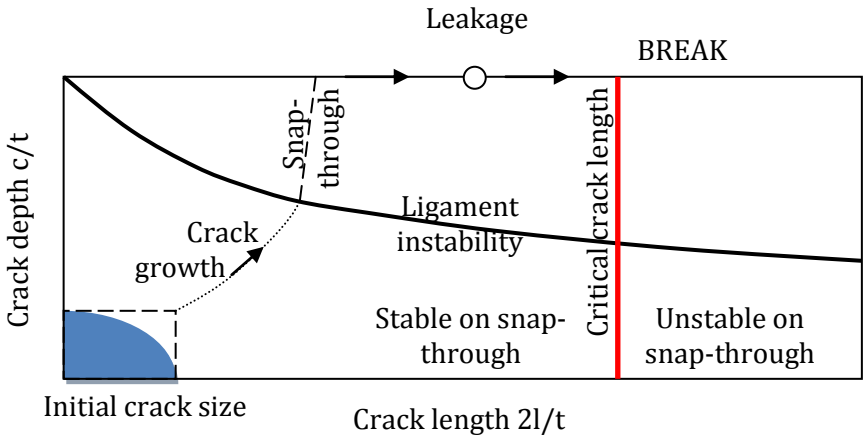

1.3-1 Scenarios of crack propagation until breakthrough

As a Leak-Before-Break argument can only be made for a through-wall crack, it is first necessary to prove that a surface crack in the case considered will penetrate the thickness of the component prior to becoming unstable and that no long surface crack formation will occur.

Diagram 1.3-1 describes the different possible scenarios of crack growth with regards to Leak-Before-Break analysis. Consider a crack of dimensions accounted for by its depth a and semi-length l in a part of a component of thickness t used as a normalising parameter. During crack growth, these dimensions may vary depending on the loading conditions to which it is subjected and the kind of propagation considered. The critical length l_c and crack propagation of a defect can be assessed by using standard R6 procedures. When the crack depth becomes important compared to the total thickness, and its length is sufficient, the remaining un-cracked part of the structure lying ahead of the crack in its mean plane, called

ligament, can be subjected to instability, and the crack depth will dynamically snap through the entire thickness. If this happens under the critical length, the instability will lead to a stable through-wall crack as shown. If it happens above the critical length, the component will break. The LBB argument should then demonstrate that leakage detection will occur early enough during the stable propagation of the through-wall crack so that safety measures can be taken before it reaches the critical length as shown in section 1.2.

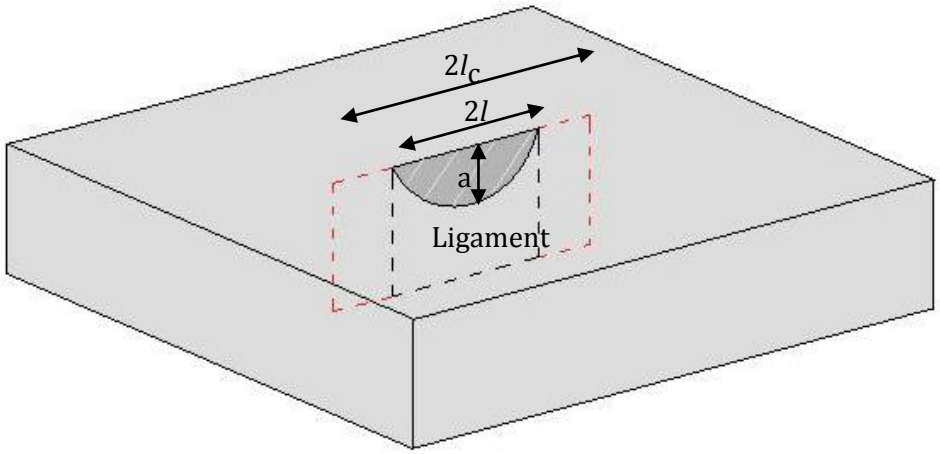

1.3-2 Configuration of a crack before breakthrough

1.4 Estimation of coolant leak rate through cracks

Several parameters need to be evaluated in undertaking LBB evaluations. Crack Opening Area (COA) of through-wall cracks is one of the most significant of such parameters as it is required for flow rate calculations in order to evaluate the size of crack at which leakage can be readily detected. They are closely related to the stress intensity factors as will be seen further.

The flow rate used in R6 is based on a model for through-wall cracks of rectangular section of width W and length L.

1.4.1 Single phase flow

Its evaluation is quite simple for a single-phase flow, and can be made in R6 through the program DAFCAT whose implemented laws are based on the following.

According to Bernoulli's law, the ideal velocity v of a fluid squirting from an orifice without charge loss from friction is given by the relation $\rho_0 v^2 / 2 = p_0$ and the flow rate is $Q = \rho_0 v A$ so that its ideal flow rate is $Q = \sqrt{2 p_0 \rho_0} A$, where p_0 is the difference between the pressures at entrance and exit respectively, ρ_0 is the density at entrance and A the crack opening area.

A discharge coefficient C_D lower than unity can be used to take into account the friction and express the flow rate as

$$Q = C_D \sqrt{p_0 \rho_0} WL \tag{1.1}$$

Geometry of the crack

- L is taken as an average of the length of the crack on the entrance and on the exit surfaces.
- W is taken as an average of the crack width at entrance w_0 and its width at exit w_{ex} related respectively to the corresponding crack opening area by $w_0 = A_0 / L$ and $w_{ex} = A_{ex} / L$
- d is crack divergence parameter expressed by $\left(w_{ex} - w_0\right) / 2W$
- D is the depth of the crack i.e the thickness of the vessel

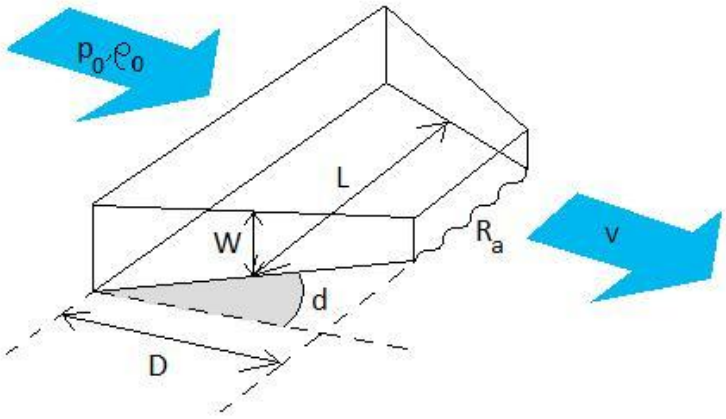

1.4-1 Configuration of a through-wall crack

Discharge coefficient

It is expressed by the mean of correlations of the general form

$$C_D = C_D\left(d, F, \frac{p_0}{p_{ex}}\right) \tag{1.2}$$

where $F = f\left(W / R_a\right) D / W$ the frictional loss coefficient depending on d in order to take into account the charge loss from a diverging or converging crack, on the dimensions of the crack W and D, on the Fanning friction factor f to take into account friction, and on

p_0 / p_{ex}. The Fanning friction factor f is a function of the ratio W over R_a the single crack surface roughness parameter. If this ratio is big, it means that there is a large opening delimited by two smooth parallel surfaces, whereas in the case of a low ratio, the defects in smoothness will not be negligible as compared to the width of the crack, so that the friction will be high.

To compute C_D, several cases are distinguished to take into account the fact that the fluid can be choked, i.e. that the fluid can go sonic if pressure is too big with low friction, the flow rate becoming critical. Thus depending on inequalities using functions of the parameters d, F and $\frac{p_0}{p_{ex}}$ obtained by correlation with experimentation, it can be choked at entrance, at exit, or unchoked.

1.4.2 Two-phase flow

For a two-phase flow of steam and water mixtures, computer programs have to be used.

In R6, the computer programs SQUIRT and PICEP are recommended. Computing critical flows only, they take into account the non-equilibrium mixture quality, the entrance pressure loss, the frictional pressure loss, the pressure loss due to acceleration arising from phase changes and changes in area, and the pressure loss due to bends and protrusion, all depending on the flow rate. Solving the pressure constraint (sum of the losses equals the total pressure drop p_0) along with the equation linking the critical flow rate to the properties of the fluid in the choking plane where it becomes critical, the flow rate can be determined.

At EDF, they are able to use ECREVISSE [3],[6] which integrates the fluid properties of saturated or out of equilibrium air/steam/water mixtures along the thickness taking into account the heat exchange, and compute the flow rate for critical or not critical flows by an iterative process. This is described in more detail in section 3.2.1.

1.4.3 Difficulties in the evaluation of leak rate for leak before break arguments

The main difficulty arises from the determination of the friction factor. First of all the surface roughness parameter R_a is difficult to evaluate from the interpretation of measures depending on many parameters, so that sensitivity analysis must be undertaken to see if the imprecision can have an severe effect on the flow rate. In this case, lower bound values should be taken in order to minimise the flow rate as described in section 1.5. In general, for artificial cracks of controlled shape and roughness, reasonable agreement is observed between measurement and theory, whereas the results are less satisfying for real cracks. For

the case of a narrow crack opening area with maximum crack opening distance (COD) in the range of 10 μm, this may be due to uncertainties in crack dimensions, particulate plugging or oxide growth blocking the passage of the fluid.

1.5 Conservatism in Leak-Before-Break arguments

Unlike most of the arguments used in assessing the fracture of a component, Leak-Before-Break arguments aim at predicting failure and not at avoiding it.

In this case, the concern of conservatism implies that the leak rate has to be underestimated, which is equivalent to underestimating the COA. As a consequence, best-estimate values of loads and material properties should be used in assessing leakage. It means that in order to minimise the results obtained in the calculation of COA, lower-bound values of loads should be taken, whereas upper-bound values of strength and yield stress should be taken.

On the contrary, pessimistic values of loads and material properties should be used in order to minimise the limiting crack length above which disruptive failure occurs. It means that upper-bound values of loads should be taken, whereas lower-bound values of strength and yielding stress should be used.

1.6 Leak detection

The choice of a suitable leak detection system must take into account the time to failure and the estimated flow rate assessed through the leak before break procedure.

There are two kinds of leak detection systems:

- The global systems include sump pumps, pumps for water systems, humidity detection for steam leaks, gas levels in air for gaseous systems and radiation monitors for nuclear systems. They detect normal leaks like valves and seals as well as incidental leaks like cracks in a large area, so that the response time to identify the source of the increase in leakage is quite long.

- The local systems include for example moisture sensitive tapes for water systems or steam systems where condensation can take place on the outer surface, and other medium which can be suitable for a specific kind of plant. These systems monitor a specific feature like a weld or a defined area.

2 Analytical approaches to the computation of COA and SIF

2.1 Evaluation of COA

There are two types of COA evaluations. One is based on Linear Elastic Fracture Mechanics (LEFM) modified by plasticity corrections. The other is using elasto-plastic models.

2.1.1 Linear elastic COA models

These models are based on linear fracture mechanics in shells enhanced by empirical formulae derived from FE calculations as functions of a few geometrical parameters.

The basis of such models is the development of stress intensity factor solutions. Here, these models are taken from [5].

2.1.1.1 Cracks under uniform loading

Consider a crack of length $2l$ in an infinite shell subjected to uniform tensile loading in mode I. The problem can be classically decomposed, by means of linearity, into the uncracked structure under tensile loading, from which an auxiliary problem is subtracted. This problem consists in the structure free of external loads except on the crack lips subjected to the uniform tensile stress.

In this auxiliary problem, Castigliano's theorem can be applied to link boundary displacements and energy, thus writing

$$A_t = \frac{1}{t}\int_{crackfaces} u_t dS = \frac{1}{t}\frac{\partial U_t}{\partial \sigma_t} \tag{2.1}$$

where t is the thickness of the shell, u_t the displacement in the direction of the tensile stress, A_t the mean crack opening area defined as the crack opening volume divided by the thickness, U_t the total strain energy in the cracked shell, and σ_t the remote tensile stress.

Then using the definition of the energy release rate G and Irwin's formula linking G and the stress intensity factor K_I, G can either be written $\frac{1}{2t}\frac{\partial U_t}{\partial l}$ or $\frac{K_I^{\,2}}{E}$, so that U_t is expressed as $2t\int_0^l \frac{K_I(l')^2}{E} dl'$. Thus finally

$$A_t = \frac{2}{E}\int_0^l \frac{\partial K_I^{\,2}}{\partial \sigma_t} dl' \tag{2.2}$$

For the particular case of an infinite flat plate with a central crack of length 2l, given that $K_I = \sigma\sqrt{\pi l}$, A_t takes the value A_0 defined as

$$A_t = A_0 = 2\pi \frac{\sigma}{E} l^2 \tag{2.3}$$

For the more general case of a thin shell of curvature $1/R$, the SIF in mode I can be expressed as

$$K_I = F(\lambda, l)\sigma_t \sqrt{\pi l} \tag{2.4}$$

where F is the bulging factor, a function of the thin shell parameter $\lambda^2 = \sqrt{12(1-\upsilon^2)}\frac{l^2}{Rt}$

Indeed, in presence of curvature, the membrane stresses tend to make the area of the crack bulge out of the structure, resulting in higher SIF.

Putting (2.4) into equation (2.2), and changing variables, the COA can be expressed as

$$A_t = A_0 \alpha(\lambda) \tag{2.5}$$

where $\alpha(\lambda) = \frac{1}{\lambda^2}\int_0^\lambda M^2(\lambda')\lambda' d\lambda'$ and where $M(\lambda') = F\left(\lambda', \frac{\sqrt{Rt}\lambda'}{\left(12(1-\upsilon^2)\right)^{1/4}}\right)$

In this way the COA is seen as its value for a flat plate corrected to take the bulging into account (bulging factor for COA).

2.1.1.2 Non uniform loading

From a more general point of view, the relationship between SIF and COA established in the last paragraph can be generalized to any plate with a centre-symmetric rectilinear crack whose edges are subjected to a centre-symmetric applied normal stress distribution with opposite direction along opposite edges. Then the stress intensity factors $K_1^{(1)}(l)$ and $K_1^{(2)}(l)$ of the same cracked body subjected to two different load cases $\sigma^{(1)}(x)$ and $\sigma^{(2)}(x)$, respectively, are interrelated according to Betti's reciprocal theorem and the superposition principle by [15]

$$K^{(1)}(l)K^{(2)}(l) = E\int_0^l \sigma^{(2)}(x)\frac{\partial u^{(1)}(x,l)}{\partial l}dx \tag{2.6}$$

where *u* is the normal crack opening displacement at coordinate x and for a semi crack length l. The crack opening area of load case 1 is defined as previously in (2.1) by

$$A(l) = 2\int_{-l}^{l} u^{(1)}(x,l)dx \tag{2.7}$$

Let the first load case be the one for which the COA is wanted and set $K^{(1)}(l) = K(l)$. Then for the second load case, the case of the uniform stress load $\sigma^{(2)}(x) = \sigma$ can be chosen so that $K^{(2)}(l) = K_u(l)$. Symmetry, and continuity at the crack tips give respectively $u^{(1)}(x,l) = u^{(1)}(-x,l)$ and $u^{(1)}(x = \pm l, l) = 0$ so that differentiating *A* with respect to *l* gives

$$\frac{\partial A}{\partial l}(l) = 2\left(u^{(1)}(l,l) + \int_0^l \frac{\partial u^{(1)}(x,l)}{\partial l}dx\right) = \frac{4}{\sigma E}K(l)K_u(l) \tag{2.8}$$

Integrating equation (2.8) with respect to *l* yields

$$A(l) = \frac{4}{\sigma E}\int_0^l K(l')K_u(l')dl' \tag{2.9}$$

For example, for a rectilinear crack in an infinite plate subjected to any symmetrical distribution of loads, using $K_I = \sigma\sqrt{\pi l}$ as the test function gives

$$A(l) = \frac{4\sqrt{\pi}}{E}\int_0^l K(l')\sqrt{l'}dl' \tag{2.10}$$

Of course, the result (2.9) could be used to find equation (2.5)

2.1.1.3 Case of a pipe under axial tension or bending moment

The nominal stresses due to tension and bending are defined by

$\sigma_t = \frac{P}{2\pi Rt}$ and $\sigma_b = \frac{M}{\pi R^2 t}$ with P and M the axial tensile force and bending moment respectively.

Consider a pipe subjected to axial tension or bending moment

- An **axial crack** will have a COA and SIF equal to zero because in the uncracked pipe, the hoop stress which could open the crack is already zero.

- For the case of a **circumferential crack under axial tension** σ_t, the stress intensity factor in mode I has the form $K_t = F_t(\theta)\sigma_t\sqrt{\pi R\theta}$ (where F_t depends on the geometry (R,t) of the pipe) and the axial stress in the uncracked pipe is uniform. So K_t can be used in equation (2.5) and change variables, and then the COA can thus be written as

$$A_t = \pi R^2 \frac{\sigma_t}{E} I_t \tag{2.11}$$

where $I_t(\theta) = 4\int_0^\theta \theta' F_t^2(\theta')d\theta'$ is a function depending on the geometry (R,t) of the pipe and θ is the crack angle, such as shown on figure

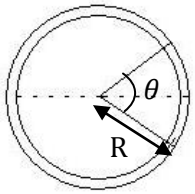

2.1-1 Definition of crack angle

- For the case of a **circumferential crack under bending moment**, the stress intensity factor in mode I has the form $K_b = F_b(\theta)\sigma_b\sqrt{\pi R\theta}$ (where F_b depends on the geometry (R,t) of the pipe) and the axial stress in the uncracked pipe is variable in the section from the most compressive zone to the most tensile zone where the axial stress is σ_b. For the most damaging case of a crack centered on the most tensile point, the SIF solution for an axial tensile stress $K_t(\theta)$ can be used as a test function $K_u(\theta)$ into equation (2.9), and then the COA can be written as

$$A_b = \pi R^2 \frac{\sigma_b}{E} I_b \tag{2.12}$$

where $I_b(\theta) = 4\int_0^\theta \theta' F_t(\theta') F_b(\theta')d\theta'$

Note that in the original paper from which these techniques are taken, results of section 2.1.1.2 are not used to determinate COA from SIF for the case of bending.

Instead of it, they used the approximation $I_b(\theta) = \frac{3+\cos\theta}{4} I_t(\theta)$ whereas the relation established here is more coherent.

2.1.1.4 Case of a pipe under internal pressure

Consider a pipe subjected to internal pressure. It can be demonstrated that the stress intensity factor in mode I can be expressed as a function of a single geometrical parameter $\rho = l/\sqrt{Rt} = \theta\sqrt{R/t}$ whereas in the case of tension or bending, the bulging factor $F(\theta)$ is different for each pipe. This is due to the fact that the membrane stresses due to internal pressure are not arbitrary anymore and take values dependant on the pipe geometry. The SIF can be expressed as

$$K_p = F_p(\rho)\sigma_p\sqrt{\pi l} \tag{2.13}$$

Under such internal pressure:

- An **axial crack** will be subjected to the equivalent of the uniform hoop stress present in the uncracked pipe, which for thin shells can be estimated by $\sigma_p = \sigma_{\theta\theta} = pR/t$. The results of section 2.1.1.1 can be used to obtain the expression

$$A_h = 2\pi Rt\frac{\sigma_h}{E} I_h(\rho) \tag{2.14}$$

- A **circumferential crack** is subject to the equivalent of the uniform axial membrane stress present in the uncracked pipe, which for thin shells can be estimated by $\sigma_p = \sigma_{zz} = pR/2t$. Results of section 2.1.1.1 can be used the same way as for the axial tensile stress

$$A_p = \pi R^2\frac{\sigma_p}{E} I_p(\rho) \tag{2.15}$$

2.1.1.5 Various models derived to compute F

- Tada and Paris (1983) model [13] : for the case of tension and bending, the bulging factor is dependant of several parameters, so the ratio R/t was set to 10 and the bulging factor was derived as development in θ/π

- Zahoor (1985) model [21]: for tension and bending R/t was taken into account in one single function used as a correction factor for terms of order more than one in the development in θ/π

- Klecker et al. [11], Lacire et al. [12], Forman et al. [4] models are based on finite element analysis and give mixed development in θ/π and R/t

2.1.2 Linear elastic COA models with small scale plasticity corrections

In an elastic body, the stresses at a crack tip are singular. Therefore, for a real material, plastic flow will occur in the vicinity of the tip. Out of the plastic zone, the stress field is well represented by the elastic solutions and indeed is increased well above the applied stress. Within the plastic zone, stress is limited by the yield stress, so that the crack tip bears less stress than in the elastic zone. As a first approximation, the crack behaves as if it is of greater length. To account for this effect, simple corrections have been developed to determinate the size of the plastic zone and correct the length of the crack.

In order to ascertain if the approximation of small scale plasticity correction is valid, an estimate of the size of the plastic zone is required.

2.1.2.1 Irwin plastic zone correction

The assumption of Irwin is that when perfect plasticity occurs at the crack tip, the distance between actual and effective crack tips should be chosen so that load not taken beyond point of effective crack tip is equal to load sustained over the distance between actual and effective crack tips.

Stresses at the crack tip are of the form

$$\sigma_{yy} = \frac{K_I}{(2\pi r)^{1/2}} f_{yy}(\theta) \tag{2.16}$$

Replacing σ_{yy} by the yield stress σ_Y when there is no out of plane stress, and solving in r for $\theta = 0$ provides an estimate of the order of size of the plastic zone i.e.

$$r_p = \frac{1}{2\pi}\left(\frac{K_I}{\sigma_Y}\right)^2 \tag{2.17}$$

In the case of a rectilinear crack in an infinite plate, equation (2.17) gives

$$r_p = \frac{l_{eff}}{2}\left(\frac{\sigma}{\sigma_Y}\right)^2 \tag{2.18}$$

Then a first correction is obtained by taking the effective crack length as $l_{eff} = l + r_p$ where r_p depends on l_{eff} through K_I. Thus this relation is implicit, and need to be solved in an iterative manner when no simple literal formulae is available for K_I.

A second estimation can be made, considering that the pressure $\sigma_{yy} = \sigma_Y$ over the effective crack tip correction size δ, is equal to the resultant of that part of the stress which is over the yield stress in linear elasticity beyond the effective crack tip, and is thus overestimated in perfect plasticity. On graph 2.1-2, these correspond to the areas A (constant yield stress pressure) and B (resultant of stress above yield stress) respectively.

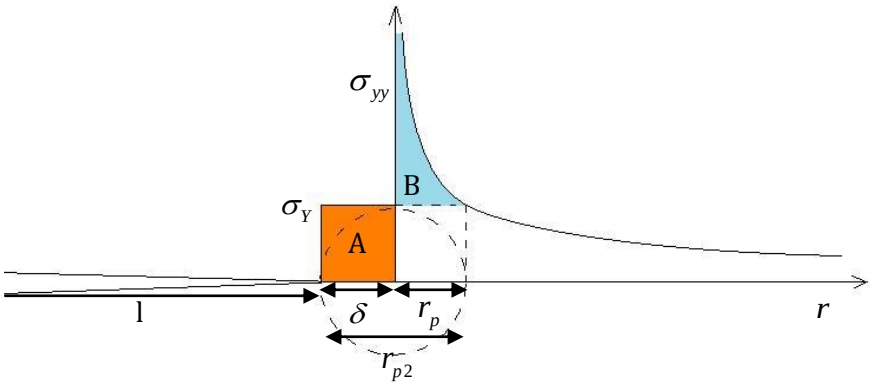

2.1-2 Irwin plasticity correction

Equating these areas yields

$$\delta\sigma_Y = \int_0^{r_p} \sigma\sqrt{\frac{l}{2r}}dr - r_p\sigma_Y \tag{2.19}$$

Thus $\delta = r_p$ and so $r_{p2} = 2r_p$.

Irwin-like small scale plasticity correction have been developed when the stress strain law satisfies Ramberg-Osgood relation of the form [9]

$$\frac{\varepsilon}{\varepsilon_0} = \frac{\sigma}{\sigma_0} + \alpha\left(\frac{\sigma}{\sigma_0}\right)^n \tag{2.20}$$

where $E\varepsilon_0 = \sigma_0$ is a normalising stress, and where α and n are two parameters characterising the plastic strain-hardening.

Then the correction is given by [9]

$$l_{eff} = l + \frac{1}{2\pi}\left(\frac{n-1}{n+1}\right)\left(\frac{K(l_{eff})}{\sigma_0}\right)^2\left(1+\left(\frac{P}{P_0}\right)^2\right)^{-1} \tag{2.21}$$

where P is the load and P_0 the limit load in perfect plasticity for the structure. Far from the limit load, for very high values of n and $\sigma_0 = \sigma_Y$, equation (2.21) reduces to Irwin's correction for perfect plasticity.

In R6, the COA is evaluated with a first order correction in σ/σ_Y by Kastner et al. [8] for the effects of crack tip plasticity [9]

$$A = A_0\alpha(\lambda)\left(\left(1+S^2/2\right)^{3/2} - \left(S^2/2\right)^{3/2}\right) \tag{2.22}$$

with $S = \frac{\sigma}{\sigma_Y}$ the loading level, ratio of membrane remote stress to flow stress

2.1.2.2 Dugdale plastic zone correction

In Dugdale's approach, the plastic zone size is the length over which a uniform pressure $-\sigma_Y$ on the faces of the effective crack should be applied to nullify the stress intensity factors. In this way the size of the plastic zone compensates exactly the loss of stress magnitude due to plasticity in this area. Formulae are readily available to compute the SIF for a crack whose edges are subjected to wedge forces, hence it is possible to integrate to obtain SIF for piecewise constant pressure [5]

$$K_I = \frac{\sigma_Y}{\sqrt{\pi l}}\int_l^{l+r_p}\left(\sqrt{\frac{l+x}{l-x}}+\sqrt{\frac{l-x}{l+x}}\right)dx = 2\sigma_Y\sqrt{\frac{l+r_p}{\pi}}\arccos\left(\frac{l}{l+r_p}\right) \tag{2.23}$$

Substituting this equation into $K_I = \sigma\sqrt{\pi\left(l+r_p\right)}$, gives

$$r_p = \frac{\pi^2 l_{eff}}{8}\left(\frac{\sigma}{\sigma_Y}\right)^2 \tag{2.24}$$

For small values of the ratio σ/σ_Y, the correction of Irwin and Dugdale are very similar. For higher values, they tend to be different, and accuracy diminishes for both methods for large scale plasticity.

2.1.3 Elastic-plastic COA models

Non-linear fracture mechanics feature two different kinds of approach to compute the COD and J integrals when plasticity is considered [9], which are described in the following paragraphs

2.1.3.1 COD estimates based on GE/EPRI (General Electric/Electric Power Research Institute) approach

This first estimation scheme uses the material properties under the form of the Ramberg-Osgood relation in which the stress strain law, fitting experimental data, is represented in the form of equation (2.20)

Then the COD is expressed by the sum of two terms: the first one δ_e is the COD in linear elasticity for a crack of the effective length accounting for small scale plasticity as described before, and which can be calculated using techniques of section 2.1.1; the other term is a corrected fully plastic solution, δ_p, depending on α and n, and taking the actual crack length as a parameter, accounting for large scale plasticity [9]

$$\delta(l,P) = \delta_e(l_{eff},P) + \delta_p(l,P) \tag{2.25}$$

where l_{eff} is the effective half-length using existing Irwin corrections for non-perfect plasticity, and P is the load.

Unfortunately, for this kind of model, it is necessary to fit experimental data with a relation that has no physical origin. Therefore, there are several ways to match the data with the three parameters, and results can significantly depend on the chosen stress σ_0 and on the range over which they have been fitted. Nevertheless, it is recommended to fit the data for small strain range using engineering stress-strain data, because for large strain range, the strain rate usually becomes more significant, resulting in the Ramberg-Osgood power law being less relevant. Using consistent definitions of parameters with regards to stress-strain data, a unique set can be obtained for a given materiel and several authors have suggested more robust schemes based on this approach.

2.1.3.2 COD estimates based on reference stress approach

This is the approach adopted by many defect assessment methods like R6.

In this approach, the ratio of total COD over elastic COD is then expressed as a function of σ_{ref} and ε_{ref} respectively the reference strain and the reference stress, and expressed with a strain hardening exponent *n* comparable to the Ramberg-Osgood form.

The reference stress is defined by $\sigma_{ref} / \sigma_Y = P / P_0 = M / M_0$ where σ_Y is the yield stress, P and M are respectively the load and moment, and P_0 and M_0 are respectively the limit load and moment in perfect plasticity. The fundamental difference with GE/EPRI scheme is that the reference strain ε_{ref} can be determined from the true strain at the reference stress σ_{ref}, thus using directly real tensile stress-strain data. Furthermore, the strain hardening exponent n is estimated using the true ultimate strain and stress from real tensile stress-strain data. For large strain range, the results are different using engineering or true stress-strain data, but the use of true stress-strain data underestimates the COA. Therefore the reference stress approach is recommended for LBB assessment.

When no full data is available, alternative schemes can be adopted to use only the true ultimate stress.

2.2 Comparison of numerical tools to address leak-before-break cases

The purpose of this study is to compare the results of the codes Abaqus [1] and Code_Aster [2] for the linear elasticity computation of local energy release rate G and local stress intensity factor K_I along the straight vertical front of a planar through-wall centred crack in a finite square plate subjected to remote traction in mode I. The crack opening areas are also compared.

2.2.1 Model

The dimension of the plate and the crack in this benchmark are the following:

- Plate width and length: 200 mm
- Plate thickness: 10 mm
- Semi-crack length: 20 mm

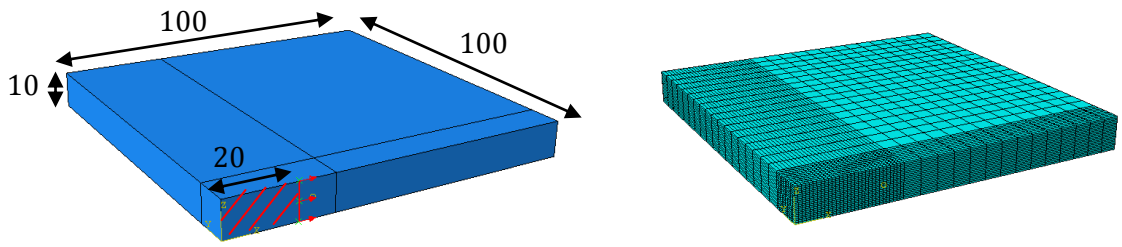

2.2-1 Geometry, definition of the crack, and mesh

For simplicity, the geometry has been meshed with quadrangles only, with a refinement around the crack surface and in the thickness of the plate. Taking into account the two

symmetry planes in this case, only a quarter of the plate has been modeled, with corresponding constraints (see 2.2-2 model a). The surface opposite to the crack surface is subjected to traction stress of 100 MPa. The remaining surfaces are stress-free. Also another mixed shell and 3D model has been created to approximate infinite plate results (see 2.2-2 model b).

The isotropic material used for the study has a Young modulus of 198000 MPa and a Poisson's ratio of 0.3, and the computations have been performed in linear elasticity.

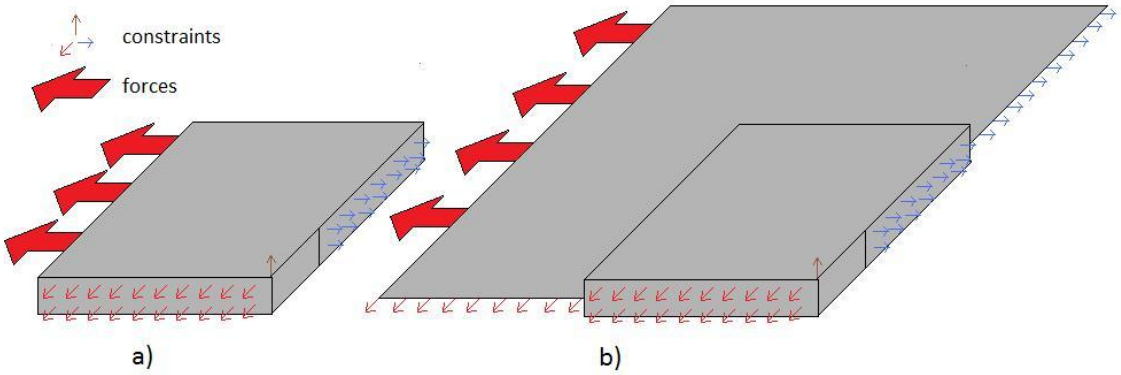

2.2-2 boundary conditions: a) finite 3D plate model b) extended mixed shell and 3D model

2.2.2 Post-processing

For symmetry reasons, there are two zero stress intensity factors $K_{II} = K_{III} = 0$.

In linear elasticity, the J-integral is path-independent and the local SIF are well defined to characterize the asymptotic development of the stress field at the crack tip so that the comparison is easy to make as theoretically the same values should be returned whatever the shape of the domains chosen to compute them.

The study has been undertaken with both linear and quadratic elements with linear elasticity only. The method which has been chosen to compute the local SIFs and G in both Code_Aster and Abaqus is based on the bilinear form of G using a virtual crack extension field whose track along the crack tip has been interpolated on its shape functions (CONTOUR INTEGRAL, TYPE=J-INTEGRAL in Abaqus, CALC_K_G with option LISSAGE_THETA (or G) = LAGRANGE in Code_Aster). Because of numerical inaccuracies on elements representing the stress singularity at the crack tip, the computations have been performed with several different contours, and the values of G and K_I have been taken from the farthest contour provided that the values on other contours were converging towards it.

The crack opening area is calculated by an integral of the y-displacement along a particular path at level z in the thickness

2.2.3 Results

Under the previously defined boundary conditions, the (amplified) deformed shape is the following

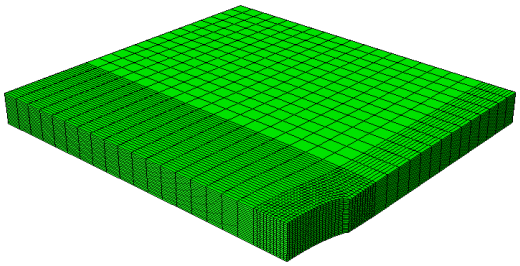

2.2-3 Deformed shape

Because in homogenous isotropic linear elasticity the fields along the 3D crack tip are equivalent to plane strain configuration, the following relation stands

$$G = \frac{1-\upsilon^2}{E}\left(K_I{}^2 + K_{II}{}^2\right) + \frac{K_{III}{}^2}{2\mu} \tag{2.26}$$

An integral form of this equation is used to compute the SIFs distinguishing by means of linearity the three loading modes of the crack, so that this relation should be verified.

The results of the analysis are represented in the following charts.

From figure 2.2-4 it can be observed that with linear elements the results are very similar. They differ of less than 2% except on the three nodes nearing the free surfaces. Code_Aster solution is oscillating near the surface. This is due to problems related to the processing of the crack tip end (oscillation because of interpolation) which has been solved by taking the mean between the values at the two neighbouring nodes, which is obviously not valid for a free surface end of a crack. The local energy release rate G obtained from stress intensity factors using equation (2.26) corresponds to the computed G.

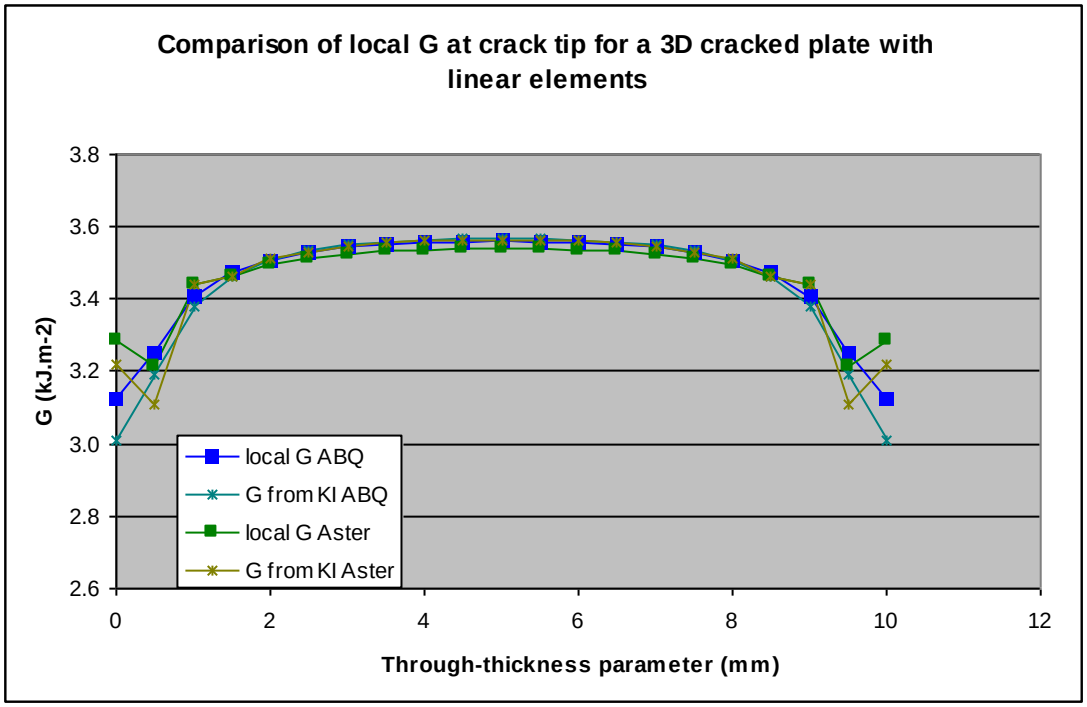

2.2-4 Comparison of local G at crack tip for a 3D cracked plate with linear elements

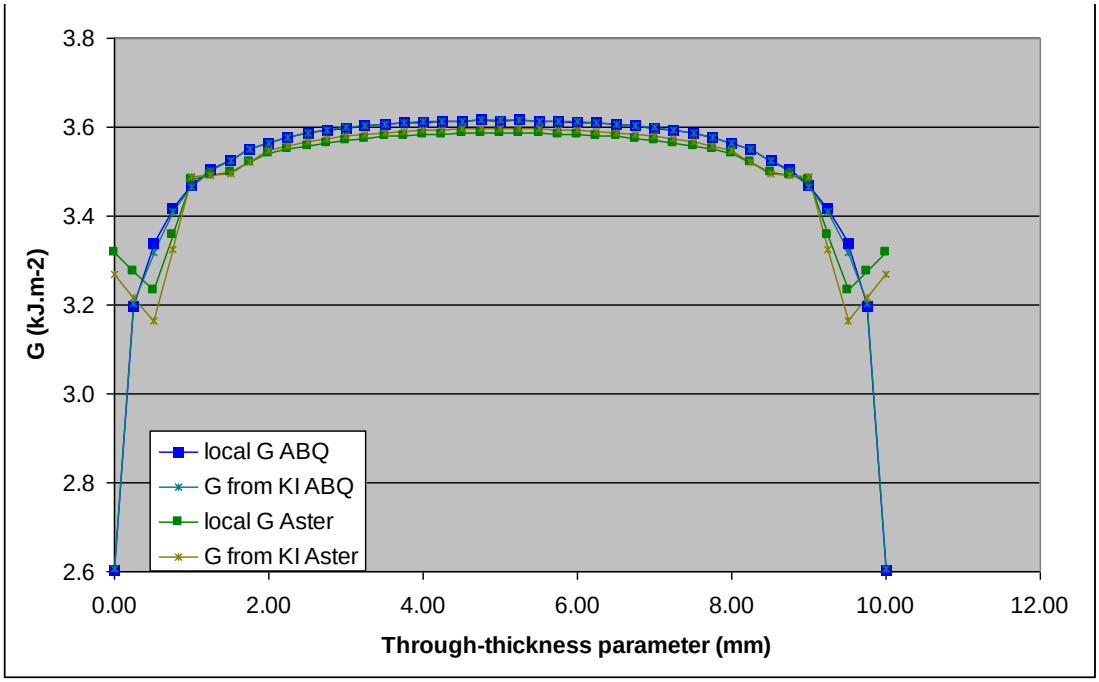

2.2-5 Comparison of local G at crack tip for a 3D cracked plate with quadratic elements

From figure 2.2-5 it can be observed that with quadratic elements all the graphs differ of less than 2% except on the three nodes nearing the free surfaces. Code_Aster solution is still not monotonous near the surface for the same reason. The local energy release rate G obtained from stress intensity factors fits well as expected. The shape observed is due to tridimensional stress effect in thin plates, part of the singularity on the surfaces coming also from out-of-plane stress.

Another study has been performed with Abaqus prolonging the 3D plate with shell elements in order to approximate the remote tensile stress in an infinite plate without using too many degrees of freedom (model b).

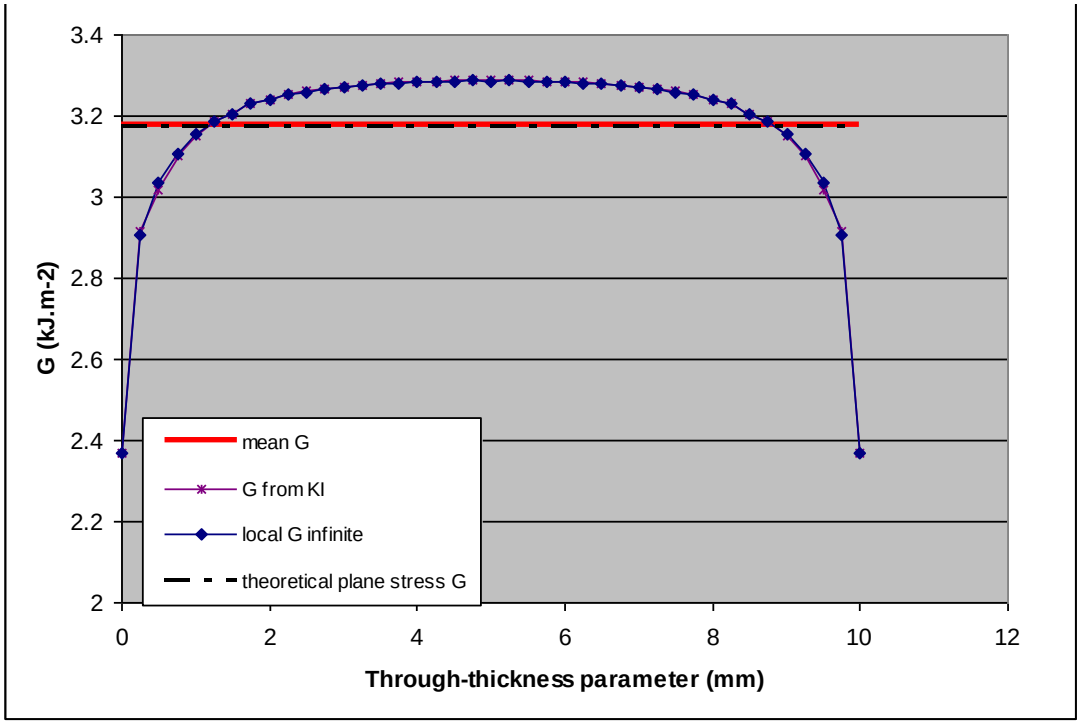

2.2-6 Local G at crack tip for a 3D cracked plate with quadratic elements with Abaqus

The result in Figure 2.2-6 is satisfying as the mean of G across the thickness fits exactly (less than 0,5%) the theoretical expression of plane stress G used for a shell approach

$$G = \frac{K_I^{\,2} + K_{II}^{\,2}}{E} + \frac{K_{III}^{\,2}}{2\mu} \tag{2.27}$$

As far as the crack opening area (COA) is concerned, it is almost constant in the thickness due to the tensile stress imposed, and the results for Abaqus and Aster with linear elements are very similar: 0,327 mm² on the free surface for Aster, and 0,330 mm², less than one percent. Given that the COA has been defined using the y component of the displacement in the first order approximation, this difference is negligible. Figure 2.2-7 shows the crack opening for the tested case obtained with linear elements. The classical elliptical shape of a crack opening under uniform tensile stress can be observed.

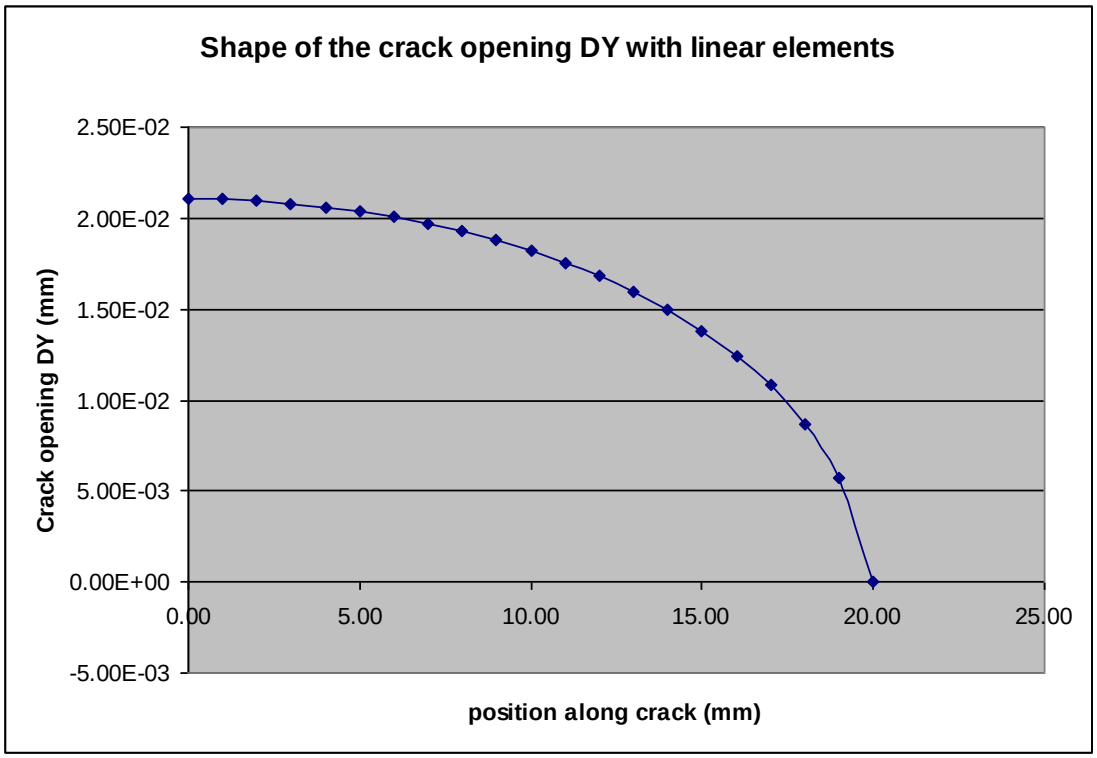

2.2-7 Shape of the crack opening

2.2.4 Conclusion

The results are satisfyingly similar using the same numerical G-θ method. Care is recommended with the use of Code_Aster for the computation of local SIF on free surfaces, where an arbitrary correction is made to compensate for regularity problems on the extremities of the crack tip. Abaqus being a commercial software, the method of discretising the G-θ method to obtain smoother and more accurate results is not discussed in the theory manual [1]. Nevertheless, the differences pointed out are only of a few percent so that the two softwares can be used to perform this kind of analysis.

3 Influence of the fluid leaking through a crack

The goal of the present study is to assess the effect of the fluid leaking through the crack on the COA and on the stress intensity factors. This assessment is to be performed by means of the thermo-mechanical coupling between the metallic component and the fluid which subjects it to pressure and thermal loading. The leaking fluid creates a variable pressure in the crack which tends to increase the COA, and transports enthalpy that it can release by heating its surfaces which in turn can swell. This effect is never taken into account in LBB assessment, because it seems that it is legitimate to neglect it for most applications.

3.1 Why take a coupling into account?

3.1.1 Influence of pressure

Let us consider a cylindrical component of thickness small compared to its radius under pressure with a circumferential crack. In the un-cracked component, the integral of the tensile stress in the direction of mode I (that is along the axis of the cylinder) is proportional to the internal pressure and the ratio radius over thickness

$$\sigma_{zz} \simeq p_0 \frac{R}{2t} \tag{3.1}$$

Considering the auxiliary problem referred to above, the effect of a constant pressure on the crack surfaces for a thin shell is the same as the effect of a remote tensile stress of equal amplitude. If the singular head loss at the entrance of the crack is neglected, and take the mean pressure throughout the thickness for a perfect incompressible fluid, the mean value between the outside and inside pressures is given by $p_0/2$.

Thus in this simple case the ratio of the crack opening stresses caused by the internal pressure and the one caused by the fluid pressure in the crack is equal to R/t. The thin shell approximation is valid only for ratios R/t approximately greater than 10, but in many cases this ratio is smaller, which could indicate that the effect can be greater than 10% and should be accounted for.

In cases where the ratio is smaller, the tensile stress in the thick shell as well as the pressure decreasing inside the crack cannot be taken into account simply by their mean across the thickness.

3.1.2 Influence of temperature

The effect of the temperature gradient is likely to have an influence on COA and stress intensity factors, depending on the different convection coefficient between the wall and the fluid, which in turn depends on the fluid considered. The fluid heats the structure which is consequently subject to thermal expansion.

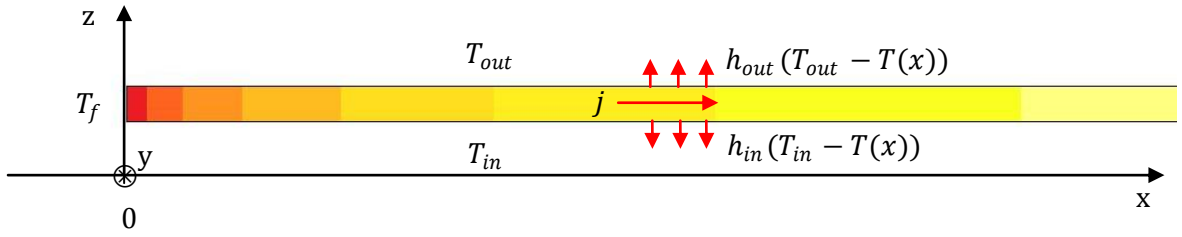

3.1-1 Description of the "fin" 1D-problem

Consider the following 1D problem. A plane shell, semi infinite in x direction ($x \geq 0$), uniform along the y axis and in its thickness in direction z, with thermal conductivity *k*, is traversed by a heat flux, *j(x)* being the scalar representing the average longitudinal flux (W.m^{-2}) in the thickness of the shell. The lower face is subjected to a temperature T_{in} and a convection heat transfer coefficient h_{in} (W.m^{-2}.°K^{-1}) of the fluid inside the component, whereas the upper face is subjected to the corresponding conditions described by the subscript *out*. The border (x=0) of the shell represents the crack surface and is subjected to the average temperature T_f and convection coefficient h_f of the fluid flowing through the crack. Between x and x+dx for a steady state, the total heat flux must be equilibrated to zero, thus

$$t(j_x(x+dx)-j_x(x))+dx(h_{in}(T(x)-T_{in})+h_{out}(T(x)-T_{out}))=0 \tag{3.2}$$

And if dx tends to 0,

$$\frac{\partial^2 T}{\partial x^2}-\left(\frac{h_{in}+h_{out}}{kt}\right)T=\frac{h_{in}T_{out}+h_{in}T_{out}}{kt} \tag{3.3}$$

Given that the temperature is not increasing with x, it can be expressed as a decreasing exponential

$$T(x)=A\exp\left(-\sqrt{\frac{h_{in}+h_{out}}{kt}}x\right)+T_{\infty} \tag{3.4}$$

Where A and T_{∞} are undefined constant temperatures to find with the boundary conditions as follows.

The condition at x=0 is $j_x(0) = -k\frac{\partial T}{\partial x}(0) = h_f\left(T_f - T\right)$ and the remote temperature can be obtained, to give

$$A = \frac{h_f T_f}{h_f + \sqrt{\frac{k(h_{in} + h_{out})}{t}}} \quad \text{and} \quad T_\infty = \frac{h_{in}T_{in} + h_{out}T_{out}}{h_{in} + h_{out}} \tag{3.5}$$

The characteristic distance over which T decreases towards T_∞ is $\delta = \sqrt{\frac{kt}{h_{in} + h_{out}}}$

If h_f is a lot bigger than the square root term in (3.5), which is very likely due to the fact that the fluid flowing through the crack has a high velocity because of high internal pressure, then $A \simeq T_f$.

With values used in the case considered in section 3.2.4, the characteristic distance is 20cm! So this kind of leak could easily be detected with temperature detectors such as infrared systems.

3.2 Thermomechanical coupled model with Aster

In order to solve coupled thermo-mechanical fluid-solid problems involving cracks, utilisation is made of a macro-command, developed by the Code_Aster team, which calls in the 1D fluid code Ecrevisse.

3.2.1 Solving the fluid problem

The ECREVISSE code [3],[6] has been primarily developed to assess leakage through tubes of steam generators of nuclear plants. It can compute the stationary leak flow rate and the thermodynamical variables of an air/steam/water mixture through a channel of variable section (for example a crack) linking two tanks where the remote fluid is considered to be still. Water (in or out of thermodynamical equilibrium) can vaporize, or steam can condense, along the channel. The main hypotheses are that the fluid is perfectly homogenous in the orthogonal section plane of a rectilinear path, the flow is stationary, and the components have the same velocity and temperature. The thermodynamical and mechanical variables (pressure, temperature, velocity, mass and volume fraction, convection coefficient) are integrated along the axis of the channel by means of the following equations: conservation of mass, conservation of the quantity of motion, conservation of energy, and the equations of state of the components involved.

The method to determinate the unknown flow rate used to solve the differential equation system is an iterative process based on the possible-impossible flow principle. The flow rate is adapted iteratively from a calculated maximum so that the pressure at the end of the channel fits the given exit pressure. If in the end the determinant of the system takes the value zero at one point of the channel, it means that the velocity of the compressible fluid is the speed of sound and that the flow rate is critical i.e. cannot increase.

3.2.2 Coupling a thermomechanical problem and a fluid problem

In Code_Aster, coupling macro-commands have been developed in order to take into account both the impact of the cracked material behavior on the flow, through the modification of the crack geometry and wall temperature, and the impact of the flow on the cracked material behavior, through the mechanical (pressure) and thermal (heat flux) stresses the flow creates in the crack vicinity.

It has been first used to assess leaks across through-wall cracks and pores of concrete containment building in French REP1300, due to the release of hot high-pressured steam during a loss of primary coolant accident [6]. In this case the coupling was modelled in 2D because the interest was obtaining the leak rate only. In the case of LBB, it is necessary to be able to model a real crack and not only two walls so it is required to couple Ecrevisse with a 3D thermomechanical model. For this purpose, a previous student created a model of a cracked pipe, modified somewhat the macro-command files in order to simplistically take into account the tri-dimensional geometry of the crack, and wrote the loop to solve the coupling (which hadn't been fully integrated in the code by the Code_Aster team)

3.2.3 Macro-Commands and principles of the coupling

3.2.3.1 How to run the case in Aster

The model is now working with the latest Code_Aster version V10. In order to run the case however, development files are still necessary to overwrite the standard version of the code, because it has been partly adapted for features particular to LBB. These features haven't been included and released in the standard version because there has not been a demand for LBB coupling in a 3D models coming from institutions performing safety studies like the SEPTEN (EDF).

In order to run the case the following is needed:

- **Ecrevisse.exe**, the executable file for Ecrevisse. Only this file is needed, it's a binary version of Ecrevisse for Linux 32 bits or 64 bits, so its sources are not required

- **The source directory** containing the python macro-command: **macro_ecrevisse.py, calc_ecrevisse.py and macro_ecre_calc.py**. In order to use them to overwrite the

previous versions of these commands, a complete installation of Aster is required. These files must be added in ASTK, the interface software of Aster, as development files. This way a python executable is created and added with symbolic link towards the standard version of Aster.

- **The capy directory** containing the capy files checking the syntax of the commands present in the python source files. As they have been changed for the purpose of the study, they are needed as development files to overwrite the standard version of Aster.

- The cases containing **a mesh file** (.mgib or .med) and a **command file for Aster** (.comm)

- The file in use in **ASTK** specifying the data and results files for the case (.astk)

3.2.3.2 Study file

This file is the usual file (.astk) needed to run a case in Aster and read by ASTK, it enables the program to access the different files for data and results.

3.2.3.3 Macro_ecre_calc.py

This macro-command writes the input data file for the fluid problem, calls Ecrevisse.exe to solve it and yields the results in a table.

3.2.3.4 Calc_ecrevisse.py

This file processes the input and output data between one time step and the next one i.e ensures the communication between the thermomechanical and the fluid problems.

- From the previous mechanical (displacement of the crack faces) and thermal (temperature on the crack faces) results, it creates the input data in use for Macro_ecre_calc

- It calls Macro_ecre_calc

- From the Macro_ecre_calc results it creates mechanical and thermal loads for the structure

This file had already been changed somewhat to take into account the 3D direction of the crack opening. In 3D, the crack opening is considered to have approximately elliptical sections. So for each point of the crack line (direction of the flow), the geometry and the temperature must be specified in order to solve the fluid problem:

- the major axis is given by the crack geometry i.e. the local crack length

- the minor axis is given by the crack opening displacement taken on the line of maximum opening (coming from the mechanical results)
- For each point of the crack line, the imposed temperature for computation of the heat exchange is given by the structure (coming from the thermal results)

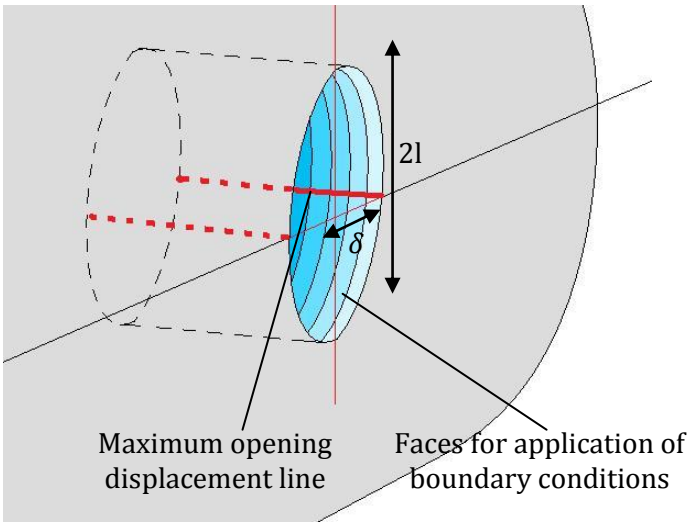

3.2-1 Geometry of the 3D crack

The thermal boundary conditions and pressure loads obtained from the fluid results were initially applied to this line as the first model was 2D, but for the purpose of a 3D study, the 1D loads have been applied on the whole crack face as a function of the position in the thickness.

This parameter is depending on the problem considered thus it is difficult to program the affectation of the load so that it works in any case. For the case of a circumferential crack in a pipe, this parameter is the radius which is not a geometrical parameter readily available in code Aster to define a field. So because of the curvature, the loads need to be defined successively on each row of face elements on the same radius.

3.2.3.5 Macro_ecrevisse.py

This file contains the Euler explicit algorithm to solve the coupling. The method is relatively simple and at each time step:

- The thermal problem is solved with some constant boundary condition (internal and external temperature and heat transfer coefficient in the case considered) and boundary condition from the fluid results on the crack surface at the previous step.
- Then the thermomechanical problem is solved with constant boundary conditions (internal pressure, tensile stress to represent the effect a pipe ends for example), boundary conditions from the fluid results at the previous step and thermal evolution from the thermal result.
- Finally the fluid problem is solved by calling Calc_Ecrevisse with the geometry of the crack coming from the displacement in the thermomechanical results and the imposed temperature along the crack coming from the thermal results.
-

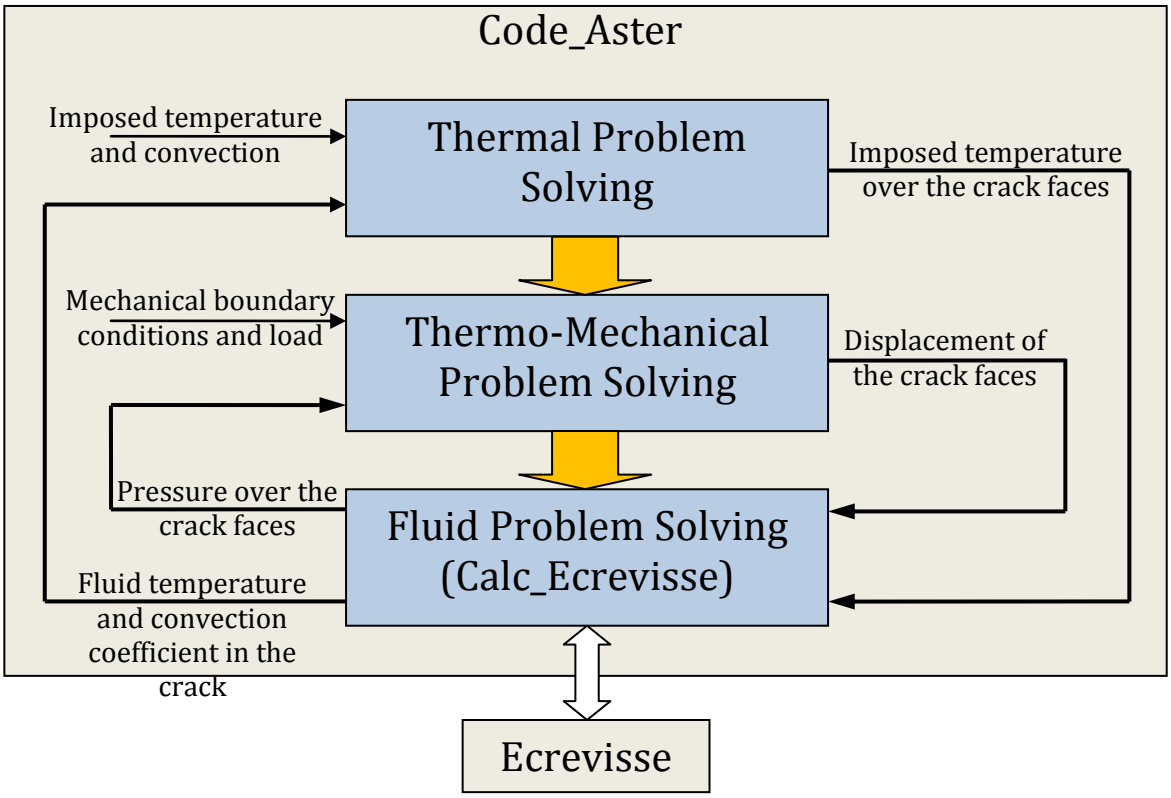

3.2-2 Structure of the loop coupling Code_Aster with Ecrevisse

It also establishes a criterion on temperature and pressure between the current step time and the previous step time to define convergence, and checks if it is verified. The loop on time steps is represented in diagram 3.2-2.

To use the macro-command, names of created concepts, properties of the fluid, models, and parameters for the criterion have to be declared:

- EXCIT_MECA and EXCIT_THER are the loads and thermal boundary conditions except on the crack faces
- CHAM_MATER and COMP_INCR defines the material field and the kind of incremental law of behavior considered
- OUVERT_REMANENTE can be used to say that there is a remaining opening area even when the crack is supposed to be closed
- LOGICIEL keyword indicate the Ecrevisse executable localisation

The crack parameters are given in the FISSURE paragraph with these keywords:

- ANGLE is the angle with the vertical axis (90° means no gravity)
- RUGOSITE indicate the surface roughness of the crack faces

- GROUP_MA are the mesh group for the line on which the COD is read, and the face of the crack on which the loads and thermal boundary conditions from the fluid are applied
- SECTION define the crack opening geometry
- DIRECTION is the crack direction i.e the direction of the fluid jet.
- DIR_OUVERTURE is the crack opening direction
- LISTE_VAL_BL are values of the crack length

The fluid parameters are given in the ECOULEMENT paragraph with these keywords:

- PRES_ENTREE indicate the entrance pressure
- PRES_SORTIE indicate the exit pressure
- FLUIDE_ENTREE indicate which fluid is considered (here 6 is air only)
- TITRE indicate the exit pressure
- PRESSION indicate the air partial pressure
- TEMP_ENTRE_FO indicate the entrance temperature

The method and the convergence criterion is defined in the CONV_CRITERE paragraph.

- TEMP_REF and PRES_REF define the reference temperature and pressure to whom the difference of temperature and pressure between to time stamps will be compared. PREC_CRIT is then the error rate.
- CRITERE defines the method. In the present work the criterion CRIT='PERMANENT' has been added with a MAX_ITER option to enable a fast convergence towards a steady-state solution, on the contrary to 'TEMP_PRES' which subdivides the time steps over the whole evolution out of thermal equilibrium, or 'EXPLICITE' which only takes the required steps without any criterion.

For the heat transfer and the friction, the models are defined in the MODELE_ECRE paragraph. See Ecrevisse documentation [3] for more information about the models.

In the CONVERGENCE paragraph the convergence criterion is defined in Ecrevisse.

3.2.3.6 Capy files

These files are required to define the syntax of the macro-commands in Aster. They had to be modified somewhat so that the user can define the direction of the flow, the direction of the crack opening and the face on which to apply the loads, required by a 3D case.

3.2.3.7 Mesh files

Meshes for the study can be generated automatically from given dimensions. For the pipe under internal pressure and temperature, there are two meshes:

- The one that had been done for the initial pipe model is a refined volume part containing a crack, linked with a shell in order to represent the pipe with less degrees of freedom. The file written in gibi development language is used by Castem to generate the mesh in mgib format. This can be done through ASTK.

- The other file is a fully tridimensional model with a converging refined mesh at the crack tip suitable for the computation of fracture mechanics features. It is generated by the mesher and post-processor Salome.

3.2.3.8 Command files

These files are the two usual files needed to run a case in Aster and must be added in ASTK as study files (.comm)

These have been separated into two files: the description of the case, and the post-processing.

Description of the case

In the first part of the first file the mesh is read, modified, groups of element are created:

- For the case with a shell part, the mesh composed of triangles with three nodes is converted into triangles with seven nodes in order to accommodate shell elements

- New groups of elements and groups of nodes are defined for boundary conditions and post processing features, especially on the crack tip and faces, and for the case of the shell model, groups are defined to link the volume and shell parts

In the second part the mechanical and thermal models are defined as well as the operating conditions parameters for the study, and the boundary conditions and loads not depending on the step are given.

In the last part, the macro-command Macro_Ecrevisse is called, taking the boundary conditions and loads as arguments, and proceed to the computation of the thermomechanical coupled study.

Post-processing

In this file the displacement and temperature fields are extracted, as well as the average displacement of the edges of the crack respectively on the inside and outside surfaces. The energy release rate and local SIF on the crack front are computed by means of the G-theta method for virtual velocity fields defined on concentric cylinders of different radii (see section 3.4).

3.2.4 Description of the model used for the coupling

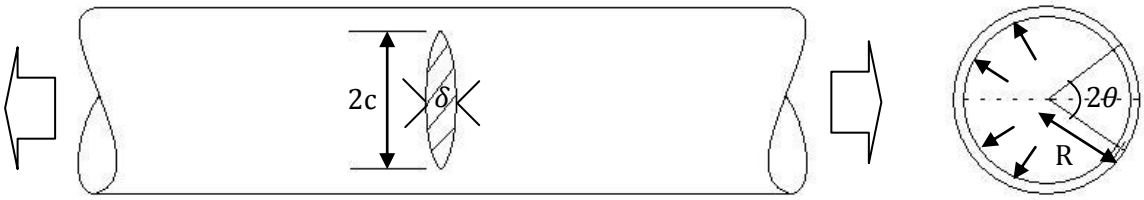

3.2-3 Geometrical configuration of the pipe model for the coupling

The model used to study the coupling of a crack and the fluid leaking through it (whose first design was done by a previous student) is a pipe with a circumferential plane crack with radial crack front and all the physical parameters are representative of a high-energy gas piping in an AGR plant, specific of the United Kingdom.

3.2.4.1 Pipe Geometry

A typical geometry has been chosen here to perform the study:

- The mean radius was set to R=100mm
- The thickness was set to t=5 or 10mm to test a different ratio.
- The semi-crack angle θ was set to angles of maximum 40°.

3.2.4.2 Material properties

The study is performed in static linear thermoelasticity for a steel component. The parameters used are:

- Young's modulus E of 200 GPa,
- Poisson's ratio ν of 0.3,
- Thermal dilatation coefficient α of $10^{-5} K^{-1}$
- Reference temperature for thermal dilatation T_0 of 20°C

- Thermal conductivity k of 46 $Wm^{-1}K^{-1}$

3.2.4.3 Loads and thermal boundary conditions

The pipe and the crack were subjected to:

- Internal pressure
- Remote tensile stress to account for the effect of membrane stress under pressure
- Internal and external imposed operating temperatures
- A heat exchange following Newton's law with an imposed convection coefficient on the inside and the outside
- Local pressure of the fluid on the crack faces coupled with Ecrevisse using the previously described macro-commands
- Newton type heat exchange imposed between the fluid and the structure over the crack face, with the coefficient of convection and temperature being given by the Ecrevisse code across the thickness according to thermodynamical variables in the fluid.

The fluid flowing from the inside to the outside was subjected to:

- Internal pressure as entrance pressure and atmospheric pressure as exit pressure (with modelled entrance pressure drop)
- Inside and outside temperature as entrance and exit temperatures
- Newton type heat exchange imposed between the fluid and the structure over the crack face, with the coefficient of convection being given by the Ecrevisse code across the thickness according to thermodynamical variables in the fluid, and the wall temperature being given by temperature in the structure.
- Friction on the crack faces ruled by the roughness of the crack surface.

Instead of considering carbon dioxide, air is considered because it is the only gas taken into account in ECREVISSE. The operating conditions and properties of the fluid used for the study are given below:

Inside the pipe

- The pressure inside the pipe, P_{in}, was set to 10,6 MPa=106 bar

For the heat exchange imposed between the fluid inside the pipe and the structure, considering Reynolds number inferior to 2100:

- The temperature inside, T_{in} , was set to 550°C
- The coefficient of convection , h_{in} , was set to 8 $\mathrm{Wm^{-2}K^{-1}}$

Outside the pipe

Normal atmospheric conditions are considered so that:

- The pressure outside, P_{out} , was set to 0.1 MPa=1 bar

For the heat exchange imposed between air outside the pipe and the structure:

- The temperature outside, T_{out} , was set to 20°C
- The coefficient of convection , h_{out} , was set to 4 $\mathrm{Wm^{-2}K^{-1}}$

3.2.5 Discussion around the models hypothesis

3.2.5.1 Fluid model

A limitation of the model is that Ecrevisse is only a 1D code. For the case of a 3D through-wall crack, the definition of the sections can be a bit arbitrary since they usually have bigger dimensions that the channel length i.e the thickness.

In addition, with Ecrevisse, the area and the perimeter of each section must be defined with a simple standard shape, so limited to the use of the maximum crack opening displacement (COD) and the shape of the opening is assumed to be an ellipse like in a flat shell under tensile stress. That may not be accurate, because for the case of large circumferential cracks, the shape tends to be more of a diamond. It doesn't allow either for cracks not lying on a plane of symmetry of the structure, because the COD would be asymmetrical as well. A solution is under development amongst the Code_Aster team to compute the COA and the perimeter of each section directly from the thermo-mechanical model into Ecrevisse, but not in the scope of the coupling.

3.2.5.2 Fluid-crack interaction

Another limitation to the coupling is the fact that Ecrevisse is a code made to compute the flow rate transiting through a crack. But when the flow rate becomes critical, the mechanical and thermodynamical quantities integrated along the channel are not physical anymore, because a shock wave should be modelled.

Also for small opening areas, the results can adopt a wide range of values changing only a few parameters. This is due to the difficulty to converge in these cases. Indeed the fluid heats up the faces of the crack, resulting in thermal dilatation that tends to close it. As the crack opening area decreases, the exchange coefficient of the fluid from forced convection becomes small as well because of the low flow rate. In this case the solid can cool the fluid without gaining much temperature. Consequently the thermal dilatation decreases and the crack opening area can be greater again.

Since for a small opening the fluid is very sensitive to these changes in section and temperature, the stability of the algorithm is quite low.

3.2.6 Evolutions and Improvements brought to the model

3.2.6.1 Evolutions

The model was initially developed for an older version of Aster 9.1, so was not working properly with the up-to-date version 10. For the project the necessary modifications have been made in Macro_Ecrevisse and Calc_Ecrevisse for it to work with the latest version, both in the command file describing the model and in the macro-commands.

In order to use modified versions of the latest macro-commands, it was required to make some modifications in Macro_Ecrevisse:

- Enable the coupling Euler scheme for the particular 3D problem. For the case of the volume linked with the shell, the thermal field required to define the properties of the material needs to be obtained by projection of the thermal results separately on the volume part and on the shell part which needs special processing to obtain its mean temperature (temperature is quadratic across the thickness of the shell)

- Get all the fields necessary for post-processing. Most of the fields used during the computation were initially destroyed. In order to post-process the mechanical data for fracture mechanics, it is required to keep the thermal fields and the loads on the crack faces. In Code_Aster, the computation of energy release rate and stress intensity factors cannot be done on a model with shell parts, because it is based on the G-theta method performing integration on the whole domain. Thus for the model with a shell part the thermomechanical results had to be projected on the volume part only and recreated with the corresponding temperature field.

- Adopt a solving scheme which converges rapidly towards a steady-state solution using an explicit method (the time parameter being non-physical) as done before by the previous student. The macro-command developed by the Code_Aster team took into account an evolution of the interaction with respect to a physical time. In their

version, it was done by subdividing each time-step so that the heat flux and the pressure along the channel between two times of the Euler explicit scheme would not vary much with regard to a certain criterion. In the modified version, the criterion is only used to know when to stop the explicit algorithm, so that results at times other than the final one are not physical, but the convergence to steady-state solution is quicker. The keyword added is CRIT='PERMANENT' with a MAX_ITER option limiting the number of iterations.

3.2.6.2 Improvements of the model

The original model was a quarter circumference of a pipe, but as there is no crack on the opposite side, the symmetry conditions only allow modelling a half-circumference, so that one arbitrary node was constrained in the X-direction to avoid rigid body motion. This doesn't yield any parasite stresses as soon as the forces in the X-direction are equilibrated.

For the cylinder under internal pressure loading, a tensile membrane stress has to be considered. In this cylinder, the mean tensile stress in the direction along its axis is proportional to the internal pressure and to the ratio of the internal section area of the pipe over the pipe plain section $\sigma_{zz} \simeq p_0 R/2t$

Shell and volume model

The advantage of a shell-volume model is that it is quite a simple mesh to generate, and above all it reduces a lot the number of degrees of freedom. It is necessary to be careful about the hypothesis underpinning such a model:

- The model becomes inaccurate when the ratio radius of curvature on thickness is small
- The link between the shell part and the volume has been improved. In order to constrain the displacement of these parts by a linear relation, the previous model considered all the lines of the face of the volume part which lie along the shell normal as rigid bodies. This doesn't allow for Poisson's effect or thermal dilatation, thus modifying quantities such as stress intensity factors. So the model has been modified to take into account a more accurate link. In this one, all the lines of the face which are parallel to the shell normal will remain lines. Of course this doesn't allow for warping of the sections.

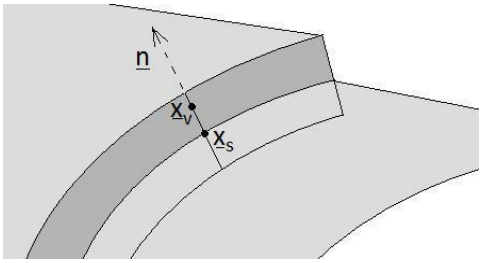

3.2-4 Link between volume and shell parts

In the following paragraph, the upper-case and lower case letters represent respectively the initial and actual configuration, whereas the subscript *v* and *s* respectively denote volume and shell. Consider the expression of the actual position of a material point $\underline{x}_i = \underline{X}_i + \underline{dx}_i$ and define $\underline{x} = \underline{x}_v - \underline{x}_s$ the relative displacement of a material point of the volume part with regard to a material point of the shell part lying on the same section.

The link was initially described for a line of nodes of the volume lying on the normal of the shell by the rigid body relation $\underline{dx} = \underline{dR}_s \times \underline{X}$ where $\underline{dR}_s$ is the rotation differential.

It was changed for the following:

- For those points of the volume part lying on the shell the constraint is $\underline{x} = \underline{0}$.
- For the other points, the rotation differential of a line of nodes of the volume lying on the normal of the shell can be written as:

$$\forall \underline{x}_v \neq \underline{x}_s \mid \underline{x} \times \underline{n} = \underline{0}\ , \quad \frac{\underline{X} \times (\underline{x}_v - \underline{x}_s)}{\|\underline{X}\| \|\underline{x}_v - \underline{x}_s\|} = \frac{\underline{X} \times \underline{dx}}{\|\underline{X}\| \|\underline{X} + \underline{dx}\|}$$

This must be equal to the shell rotation vector $\underline{dR}_s$ thus $\underline{X} \times \underline{dx} = \|\underline{X}\| \|\underline{X} + \underline{dx}\| \underline{dR}_s$

And as $\underline{dx}$ and $\underline{dR}_s$ are small, then the linear equation verified by the degrees of freedom is finally expressed as $\underline{n} \times \underline{dx} = \|\underline{X}\| \underline{dR}_s$

The elements used here are 3D elements (HEX8) with degrees of freedom DX, DY, DZ for the volume part and 2½D elements (TRIA7) with degrees of freedom DX, DY, DZ, DRX, DRY, DRZ for the shell part.

Fully tridimensional model

In the present work, a fully tridimensional model with a converging refined mesh at the crack tip suitable for the computation of fracture mechanics features has been developed. This was generated by the mesher and post-processor SALOME using development scripts. Using a judicious partitioning, the pipe was divided into blocks of hexahedral topology only with a refinement at the crack tip, so one could mesh it easily with a basic algorithm no matter

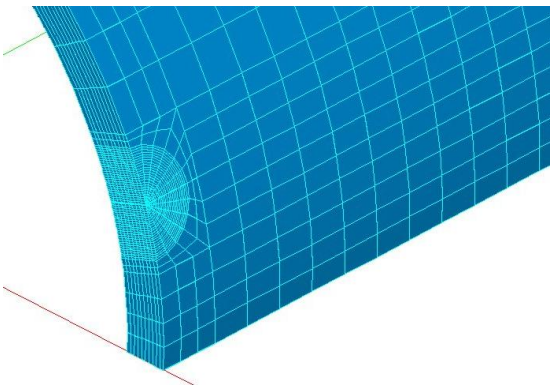

3.2-5 Example of refined 3D mesh for the crack front

which geometrical parameters are given. In this way any circumferentially cracked pipe can be generated automatically from dimensions of the pipe and the crack.

The elements used here are 3D elements (HEX8) with degrees of freedom DX, DY, DZ.

3.3 Results

3.3.1 Qualitative analysis of observed deformed state

For the pipe case with coupling, different phenomena can affect the shape of the crack opening and the distribution of stress intensity factors.

- The pressure over the crack faces tends to open the crack. In practice, it seems that this effect is not very big as compared to the effect of the thermal dilatation.

- Thermal dilatation causes the closure of the crack. It is thus in competition with the membrane stress caused by the internal pressure, and the pressure of the fluid over the crack faces.

- The bulging of the crack under tension causes a rotation of the crack faces toward the outside of the pipe. Thus, if the pipe is quite thick, there can be a difference between the inside and outside crack opening displacement, the inner one being lower than the outer one. It is not a generally important effect because the rotation is quite low, so the variation in crack opening between inside and outside is negligible as compared to the mean crack opening area, except if the effect of heating by the fluid is present. It can indeed tend to close the crack by thermal dilatation, but still accentuates its bulging. Therefore, it can for example have the effect of shutting the entrance of the crack only.

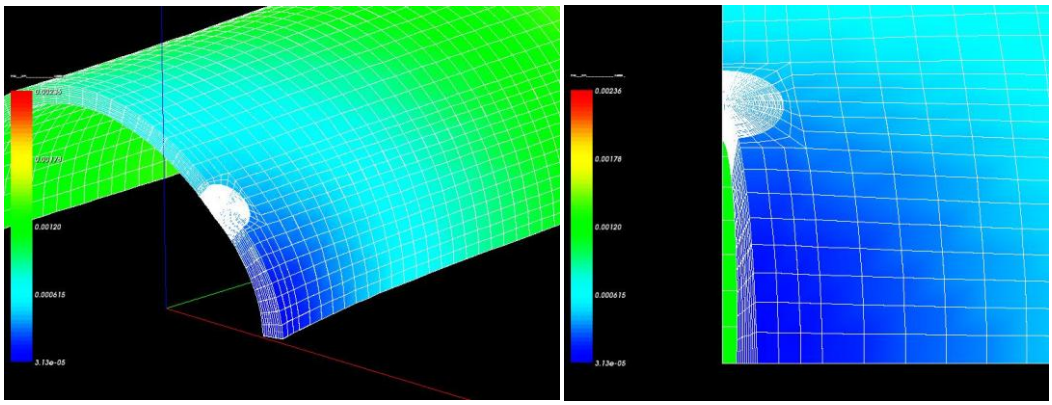

3.3-1 Deformed shape for a semi crack angle of 30°

3.3.2 Results of COA and SIF analysis

First it is of great important to note that the determination of SIF in thermomechanical analysis here has yielded some problems on which the author has struggled together with Code_Aster team.

Actually, the G-theta method (energy release rate as a volume integral of the whole domain with a virtual crack extension field of restricted support, see section 3.4) developed by Code_Aster team is not domain-independent when considering a thermomechanical stress state. This means that the cylinders defined as a support for the virtual crack extension field needs to be quite close to the crack front so that the values of the integral on two consecutives crowns may be close. First following the recommendation of the experts, in terms of cylindrical support size, the method failed to find close values, so that no value could be taken for the energy release rate.

The difference here as opposed to usual cases is that the crack is being heated on the crack face, the heat flux field is singular on the crack front and is very strong in the crack vicinity. Thus it was required to refine the mesh around the crack front a lot in order to obtain satisfyingly close values and to identify the limit of these values in the vicinity of the crack front.

In this study, a circumferential crack has been considered, and the crack angle has been set between 20 and 40°. Three sets of data have been gathered for each crack angle: first, the energy release rate without taking the fluid into account, then the energy release rate in the coupled case, and finally the energy release rate without thermal stresses, applying only the pressure from the fluid. The latter set is totally artificial and non physical, but it allows comparing the effect of temperature and the effect of pressure in the crack. Results can be seen in figure 3.3-2.

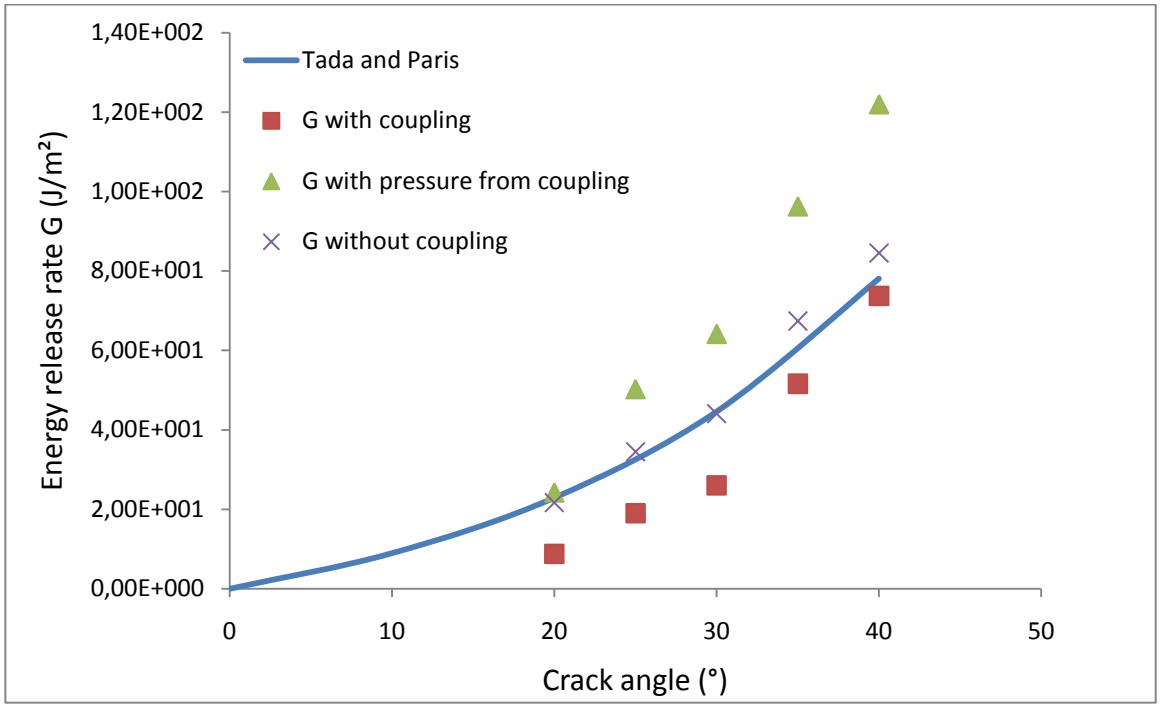

3.3-2 Comparison of energy release rates

It is very difficult to come to a general conclusion valid for any pipe and geometry, but on this particular example of dimensions, the larger the crack is, the stronger are the effects of both pressure and thermal dilatation on the energy release rate (note that this is expected for pressure at least). In this case, the influence of temperature more than compensates the influence of pressure, resulting in relative crack closure as compared to the non-coupled case. Nevertheless it is observed that the influence of temperature compensates a smaller part for higher values of angle.

Two evaluations of the flow rate have been performed: one is the result of the coupled model, and the other has been obtained by taking values of crack opening displacement for the pipe without coupling with the fluid, and entering them into Ecrevisse without considering heat exchange. For the particular configurations considered, it can be seen that the flow rate without coupling is really overestimated, thus justifying the fact that the fluid should be taken into account in a certain number of cases. For bigger angles the effect of temperature and the effect of pressure seem to compensate each other.

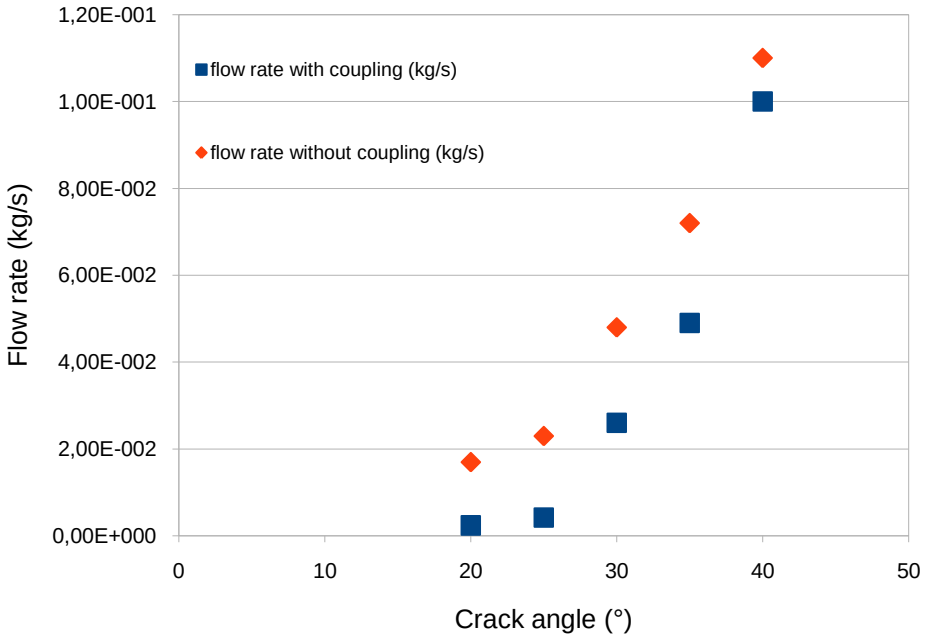

3.3-3 Comparison between flow rate with and without coupling

3.3.3 Conclusion

It is apparent that in certain cases, the influence of the coupling is not negligible. However it is difficult to give simple quantitative engineering recommendations about this effect. Where a significant influence of temperature is suspected, the present work would recommend using finite element analysis with coupling, such as made possible by Code_Aster and Ecrevisse and perform a sensibility analysis in order to adopt adequate margins.

3.4 Analytical methods for analysis of thermo-mechanical fracture mechanics problems

As it has been seen in section 3.3, the influence of temperature can considerably change the results of crack opening areas under certain circumstances. This part presents some of the analytical tools that can be used to perform linear fracture mechanics in the presence of thermal expansion.

3.4.1 G-θ Method in the presence of thermal expansion

The present section intends to describe a classic theoretical method to obtain the energy release rate G in a cracked body in linear thermo-elastics. The so-called G-θ method is here adapted to a case where thermal expansion is present. The energy release rate $G(\underline{\theta})$ is obtained by taking the negative of the differentiation of the total mechanical energy of the cracked body with respect to a propagation of parameter η of the crack tip in the direction of a virtual crack extension velocity field $\underline{\theta}$. Under certain circumstances described hereafter, the value of the field inside the body is of no importance except on the crack tip.

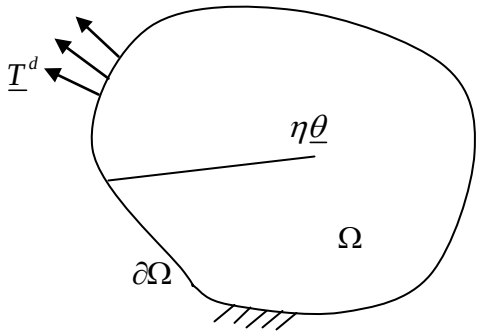

3.4-1 Cracked body

The total mechanical energy of body Ω of boundary $\partial\Omega$ in the absence of body forces can be written as

$$W = \int_{\Omega} \psi d\Omega - \int_{\partial\Omega} \underline{T}^d . \underline{u} dS \tag{3.6}$$

where $\underline{u}$ is the displacement field in the actual configuration, ψ is the strain-energy in this configuration, and $\underline{T}^d$ is an invariant field of imposed surface forces.

The expression of the free energy is

$$\psi = \frac{1}{2}\left(\underline{\underline{\varepsilon}} - \alpha T \underline{\underline{I}}\right) : \underline{\underline{\underline{A}}} : \left(\underline{\underline{\varepsilon}} - \alpha T \underline{\underline{I}}\right) \tag{3.7}$$

where $\underline{\underline{\varepsilon}}$ is the strain tensor, symmetric part of the displacement gradient, $\underline{\underline{\underline{\underline{A}}}}$ is the elasticity tensor, T is the temperature, and α is the thermal expansion coefficient.

The expression of Cauchy's stress tensor is

$$\sigma = \underline{\underline{\underline{\underline{A}}}} : \left(\underline{\underline{\varepsilon}} - \alpha T \underline{\underline{I}} \right) \tag{3.8}$$

Let $\underline{\theta}$ be a field of class $C^1(\Omega)$ piecewise, tangent to $\partial\Omega$ (including the crack faces).

Then for an infinitesimal real η, the transformation of the domain defined by

$$\begin{aligned} F_\eta(\underline{\theta}) &: \Omega \to \Omega' \\ \underline{X} &\to \underline{x} = \underline{X} + \eta \underline{\theta} \end{aligned} \tag{3.9}$$

doesn't displace the boundary except the crack front. Then $\underline{\theta}$ represents a virtual crack extension velocity field.

In such a transformation, the Lagrangian differential of a field v is expressed as

$$\dot{v} = \frac{\partial v}{\partial \eta} + \underline{\nabla v}.\underline{\theta} \tag{3.10}$$

Using moving-boundary integral differentiation, the invariance of $\underline{T}^d$ (i.e. $\dot{\underline{T}}^d = \underline{0}$), and the fact that $\underline{\theta}$ is tangent to $\partial\Omega$, W can be differentiated with respect to a crack propagation η as follows

$$\frac{\partial W}{\partial \eta} = \int_\Omega \left(\dot{\psi} + \psi div \underline{\theta} \right) d\Omega - \int_{\partial\Omega} \underline{T}^d . (\dot{\underline{u}} + \underline{u} div_{\partial\Omega} \underline{\theta}) dS \tag{3.11}$$

where $\dot{\psi}$ is the Lagrangian differential of ψ.

In linear thermo-elasticity, ψ can be differentiated as

$$\dot{\psi} = \frac{\partial \psi}{\partial \underline{\underline{\varepsilon}}} : \dot{\underline{\underline{\varepsilon}}} + \frac{\partial \psi}{\partial T} \dot{T} \tag{3.12}$$

where $\dot{\underline{\underline{\varepsilon}}}$ is the Lagrangian differential of the strain tensor.

It can be checked that $\dot{\underline{\underline{\varepsilon}}}$ is the symmetric part of $\underline{\underline{\dot{\nabla} u}}$. The double contraction of the anti-symmetric part with the symmetric tensor $\frac{\partial \psi}{\partial \underline{\underline{\varepsilon}}}$ is equal to zero so that $\dot{\psi}$ can be written as

$$\dot{\psi} = \frac{\partial \psi}{\partial \underline{\underline{\varepsilon}}} : (\dot{\underline{\underline{\nabla}}} \underline{u}) + \frac{\partial \psi}{\partial T} \dot{T} \tag{3.13}$$

where the different terms can be expressed as follows

$$\frac{\partial \psi}{\partial \underline{\underline{\varepsilon}}} = \underline{\underline{\sigma}} \tag{3.14}$$

$$\frac{\partial \psi}{\partial T} = (\underline{\underline{\varepsilon}}(u) - \alpha T \underline{\underline{I}}) : \underline{\underline{\underline{\underline{A}}}} : (-\alpha \underline{\underline{I}}) = -\alpha . tr(\underline{\underline{\sigma}}) \tag{3.15}$$

where *tr* is the tensor trace

$$\dot{T} = \frac{\partial T}{\partial \eta} + \underline{\nabla} T . \underline{\theta} \tag{3.16}$$

where $\frac{\partial T}{\partial \eta}$ equals zero if the temperature field is in a steady state. The Lagrangian differentiation of a gradient leads to

$$(\dot{\underline{\underline{\nabla}}} \underline{u}) = \underline{\underline{\nabla}} \dot{\underline{u}} - \underline{\underline{\nabla}} \underline{u} . \underline{\underline{\nabla}} \underline{\theta} \tag{3.17}$$

Substituting (3.13) into (3.12) yields

$$G(\underline{\theta}) = \int_{\Omega} (\underline{\underline{\sigma}} : (\underline{\underline{\nabla}} \underline{u} . \underline{\underline{\nabla}} \underline{\theta}) - \psi div \underline{\theta} - \frac{\partial \psi}{\partial T} \underline{\nabla} T . \underline{\theta}) d\Omega - \int_{\Omega} \underline{\underline{\sigma}} : \underline{\underline{\nabla}} \dot{\underline{u}} d\Omega + \int_{\partial\Omega} \underline{T}^d . (\dot{\underline{u}} + \underline{u} div_{\partial\Omega} \underline{\theta}) dS \tag{3.18}$$

Also, since $\dot{\underline{u}}$ is a field that is kinematically admissible it can be used as a test function in the variational formulation of the mechanical problem, thus

$$\int_{\Omega} \underline{\underline{\sigma}} : \underline{\underline{\nabla}} \dot{\underline{u}} d\Omega - \int_{\partial\Omega} \underline{T}^d . \dot{\underline{u}} . dS = 0 \tag{3.19}$$

Using (3.18) and (3.19) the expression of the energy release rate is finally obtained

$$G(\underline{\theta}) = \int_{\Omega} \left(\underline{\underline{\sigma}} : (\underline{\underline{\nabla}} \underline{u} . \underline{\underline{\nabla}} \underline{\theta}) - \psi div \underline{\theta} - \frac{\partial \psi}{\partial T} \underline{\nabla} T . \underline{\theta} \right) d\Omega + \int_{\partial\Omega} \underline{T}^d . \underline{u} div_{\partial\Omega} \underline{\theta} dS \tag{3.20}$$

3.4.2 Equivalence between the G-θ Method and a modified J-Integral in the presence of thermal expansion

Consider a flat plate subjected only to in-plane boundary forces, in which a stress-free crack is inserted, and where stress and displacement are supposed to be constant in the thickness.

It is interesting to link the G-θ Method and the J-Integral in the case of thermal expansion. As the formula of $G(\underline{\theta})$ can be used for 3D problems as well as for 2D problems, almost the same demonstration can apply from a 3D formulation to a shell J-integral or directly for a 2D problem, as long as it is supposed that the crack front is orthogonal to the shell surfaces.

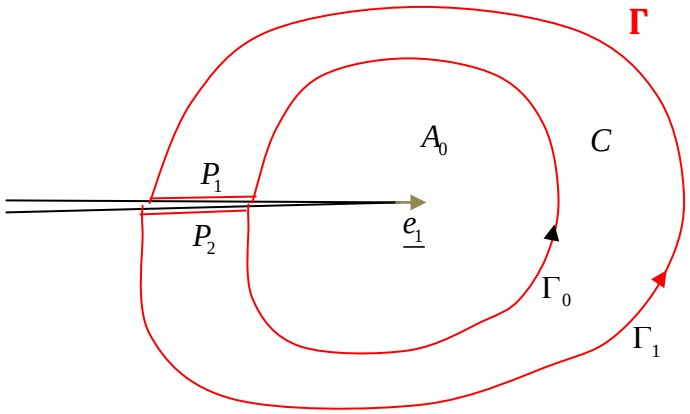

3.4-2 Definition of paths around crack tip

For this purpose a closed path $\Gamma = \Gamma_1 + P_1 - \Gamma_0 + P_2$ is defined (see fig. 3.4-2). A virtual crack extension field $\underline{\theta}$ is chosen which is equal to a constant unitary vector $\underline{e_1}$ on area A_0, tangent to the crack faces (and to the shell surfaces), invariant in the thickness, and decreasing toward zero on Γ_1, so that it is equal to zero were boundary forces are applied.

Then the second term of (3.20) equals zero, and for the first two terms of the integrand of the first term, the domain can be restricted to domain C because $\underline{\theta}$ is constant outside this zone

$$G(\underline{\theta}) = \int_C \left(\underline{\underline{\sigma}} : (\underline{\underline{\nabla u}}.\underline{\underline{\nabla \theta}}) - \psi div\underline{\theta} \right) dC - \int_\Omega \frac{\partial \psi}{\partial T} \underline{\nabla T}.\underline{\theta} d\Omega \qquad (3.21)$$

Using the equilibrium in the absence of volume force, it can be noticed that

$$div\left(\underline{\underline{\sigma}}.(\underline{\underline{\nabla u}}.\underline{\theta}) - \psi\underline{\theta} \right) = \underline{\underline{\sigma}} : (\underline{\underline{\nabla u}}.\underline{\underline{\nabla \theta}}) - \psi div\underline{\theta} + (\underline{\underline{\sigma}} : \underline{\underline{\underline{\underline{\nabla(\nabla u)}}}} - \underline{\nabla \psi}).\underline{\theta} \qquad (3.22)$$

The gradient of energy can be calculated as follows

$$\underline{\nabla \psi} = \frac{\partial \psi}{\partial \underline{\underline{\varepsilon(u)}}} : \underline{\underline{\underline{\underline{\nabla \varepsilon(u)}}}} + \frac{\partial \psi}{\partial T} \underline{\nabla T} \qquad (3.23)$$

where $\frac{\partial \psi}{\partial T}$ is expressed in (3.15) .

$$\underline{\nabla \psi} = \underline{\underline{\sigma}} : \underline{\underline{\underline{\underline{\nabla(\nabla u)}}}} - \alpha.tr(\underline{\underline{\sigma}})\underline{\nabla T} \qquad (3.24)$$

Substituting (3.23) and (3.24) in (3.22) yields

$$\underline{\underline{\sigma}} : (\underline{\underline{\nabla u}}.\underline{\underline{\nabla \theta}}) - \psi div\underline{\theta} = div\left(\underline{\underline{\sigma}}.(\underline{\underline{\nabla u}}.\underline{\theta}) - \psi\underline{\theta}\right) - \alpha.tr(\underline{\underline{\sigma}})\underline{\nabla T}.\underline{\theta} \tag{3.25}$$

Using the divergence theorem and (3.25) yields

$$G(\underline{\theta}) = \oint_{\Gamma}\left(\underline{\underline{\sigma}}.(\underline{\underline{\nabla u}}.\underline{\theta}) - \psi\underline{\theta}\right).\underline{n}d\Gamma + \iint_{C}\frac{\partial\psi}{\partial T}\underline{\nabla T}.\underline{\theta}dC - \iint_{\Omega}\frac{\partial\psi}{\partial T}\underline{\nabla T}.\underline{\theta}d\Omega \tag{3.26}$$

The crack faces P_1 and P_2 and the shell surfaces are stress-free and $\underline{\theta}$ is tangent to them. Furthermore, $\underline{\theta}$ equals 0 on Γ_1, thus, considering that the orientation of Γ_0 is opposite to that of Γ

$$G(\underline{\theta}) = -\oint_{\Gamma_0}\left(\underline{\underline{\sigma}}.(\underline{\underline{\nabla u}}.\underline{\theta}) - \psi\underline{\theta}\right).\underline{n}d\Gamma_0 - \int_{A_0}\frac{\partial\psi}{\partial T}\underline{\nabla T}.\underline{\theta}dA_0 \tag{3.27}$$

On A_0 and Γ_0, $\underline{\theta} = \underline{e_1}$, so

$$G(\underline{\theta}) = \oint_{\Gamma_0}\left(\psi\underline{n_1(\Gamma_0)} - \frac{\partial\underline{u}}{\partial x_1}.\underline{\underline{\sigma}}.\underline{n}\right)d\Gamma_0 - \int_{A_0}\frac{\partial\psi}{\partial T}\frac{\partial T}{\partial x_1}dA_0 \tag{3.28}$$

which is the J-integral corrected by an extra-term to take the thermal expansion into account.

3.4.3 Modified J-Integral in the presence of thermal expansion

This section intends to prove that the classic J-integral calculated over a closed path without geometrical singularities is equal to zero in linear elasticity, and is depending on the gradient of the temperature in linear thermo-elastics. Then a modified expression can be used, corresponding to the energy release rate, and path-independent. The expression of the classic J-integral on a path Γ enclosing a surface A is the following

$$J_{\Gamma} = \oint_{\Gamma}\left(\psi\underline{e_1} - \frac{\partial\underline{u}}{\partial x_1}.\underline{\underline{\sigma}}\right).\underline{n}d\Gamma \tag{3.29}$$

Using the divergence theorem yields

$$J_{\Gamma} = \int_{A} div\left(\psi\underline{e_1} - \frac{\partial\underline{u}}{\partial x_1}.\underline{\underline{\sigma}}\right)dA \tag{3.30}$$

The divergence can be developed using the equilibrium equation as follows

$$J_{\Gamma} = \int_{A}(\underline{\nabla\psi}.\underline{e_1} - \underline{\underline{\nabla\frac{\partial\underline{u}}{\partial x_1}}} : \underline{\underline{\sigma}})dA \tag{3.31}$$

Then using (3.24), the two terms depending on the displacement field annihilate each other, and the integral is left with a non-zero remaining part

$$J_\Gamma = \int_A \frac{\partial \psi}{\partial T} \frac{\partial T}{\partial x_1} dA \tag{3.32}$$

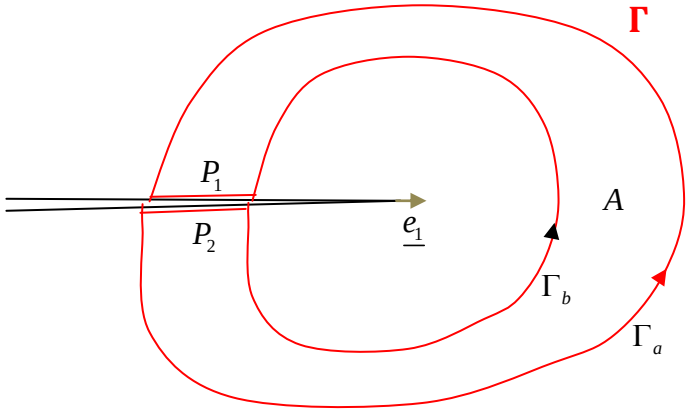

3.4-3 Definition of paths around crack tip

Then defining a closed path $\Gamma = \Gamma_a + P_1 - \Gamma_b + P_2$ (see fig. 3.4-3), it can be noted that the crack faces are stress-free and the scalar product of the normal of the path with the direction of the crack is equal to zero, so that there is no contribution to the integral from P_1 and P_2.

Finally, if Γ_b tends to the crack tip, the use of (3.32) with Γ give the path independence of the modified J-integral described by (3.28).

3.4.4 COA and SIF for a rectilinear crack heated by a uniform flux in an infinite plate with thermal exchange

This section presents an investigation on the effect of crack closure by thermal dilatation in a simpler case than the one of the cracked pipe with coupling, namely an infinite plate subjected to convectional thermal exchange on its edges, and containing a rectilinear crack whose edges are heated by a uniform flux.

3.4.4.1 Theoretical analysis

In a plate of thickness t subjected to convection thermal exchange on both faces, the membrane heat flux must equal the thermal loss by both sides of the plate, so that the heat-conduction equation for the temperature throughout the plate using Newton's law is

$$t div \vec{j} + h_+ \left(\theta - \theta_{ext+}\right) + h_- \left(\theta - \theta_{ext-}\right) = 0 \tag{3.33}$$

And using Fourier's law

$$-kt\Delta\theta + (h_+ + h_-)\theta - h_+\theta_{ext+} + h_-\theta_{ext-} = 0 \tag{3.34}$$

where θ is the absolute temperature, k is the conduction coefficient, $\vec{j}$ the heat flux, $h_{\pm}$ and $\theta_{ext\pm}$ respectively the convection coefficients and temperatures of the fluid on each side of the plate, and Δ denotes the Laplacian.

Equation (3.34) reduces to

$$\Delta T - \chi^2 T = 0 \tag{3.35}$$

where $\chi^2 = \frac{h_+ + h_-}{kt}$ and $T = \theta - \frac{h_+\theta_{ext+} + h_-\theta_{ext-}}{h_+ + h_-}$, the difference between the temperature in the plate and its value for an equilibrated plate without sources of heat.

Consider now a rectilinear horizontal crack of length 2l in plane (x, y). The plate is a domain Ω delimited by a boundary Γ composed by the two crack edges $\Gamma^{\pm}$, and a remote boundary Γ_r around the crack.

The crack lips are subjected to a uniform normal flux q, so that the boundary conditions are

$$-k\frac{\partial T^{\pm}}{\partial n}(s) = \pm q(s) = \pm q \tag{3.36}$$

with s the curvilinear parameter along the crack, and $T^{\pm}$ the limit temperature on either edge $\Gamma^{\pm}$ of the crack.

Consider the integral formulation

$$\int_{\Omega} \tilde{T}\left(\Delta T - \chi^2 T\right) d\Omega = 0 \tag{3.37}$$

where $\tilde{T}$ is a test-function.

Note that

$$div(\tilde{T}\underline{\nabla T}) - div(T\underline{\nabla \tilde{T}}) = \tilde{T}\Delta T - T\Delta\tilde{T} \tag{3.38}$$

Integrating equation (3.38) and using Green's theorem yields

$$\int_{\Omega} \tilde{T}\Delta T - \int_{\Omega} T\Delta\tilde{T} = \int_{\Gamma} \tilde{T}\underline{\nabla T}.\underline{n}d\Gamma - \int_{\Gamma} T\underline{\nabla \tilde{T}}.\underline{n}d\Gamma \tag{3.39}$$

so that substituting equation (3.37) in equation (3.39) gives

$$\int_{\Omega} T\left(\Delta\tilde{T} - \chi^2\tilde{T}\right) d\Omega = -\int_{\Gamma} \tilde{T}\underline{\nabla T}.\underline{n}d\Gamma + \int_{\Gamma} T\underline{\nabla \tilde{T}}.\underline{n}d\Gamma \tag{3.40}$$

where $\tilde{T}$ can be chosen as a zero-order modified Bessel function of second kind K_0 which is the canonical solution of equation (3.37), i.e. satisfies

$$\Delta\tilde{T} - \chi^2\tilde{T} = 2\pi\delta(x, y) \tag{3.41}$$

so that

$$T(x, y) = \frac{1}{2\pi}\left(\int_{\Gamma} \tilde{T}\frac{q}{k}d\Gamma + \int_{\Gamma} T\frac{\partial\tilde{T}}{\partial n}d\Gamma \right) \tag{3.42}$$

As Γ_r moves away from the crack, the boundary temperature and heat flux decay to zero faster than the length of the boundary, so that the corresponding integral tends toward zero. In addition, as the problem is symmetrical with respect to the x axis, the first integral yields the same value on each side of the crack, and the second integral in equation (3.42) is equal to zero, so that

$$T(x, y) = \frac{q}{\pi k}\int_{-l}^{l} K_0\left(\chi\left(\sqrt{(s-x)^2 + y^2} \right) \right) ds \tag{3.43}$$

Formulae are readily available to determine the stress state induced by a single source in an uncracked plate. Integrating these stresses multiplied by the density found previously gives the stress field induced by the total flux on path L in the uncracked plate (1*).

Then the auxiliary problem (2*) is solved consisting of the cracked plate without thermal dilatation whose edges are loaded by pressures opposite to the normal stresses obtained from the uncracked plate, in order to equilibrate them (tangential stresses are zero because of the symmetry). This non-thermal problem can be solved by means of complex Kolosov-Muskhevili potentials.

To obtain the thermo-mechanical stress state induced in the cracked plate (3*), the thermo-mechanical solution for the uncracked plate (1*) and the solution for the auxiliary problem (2*) are added by means of linearity in order to ensure stress-free crack edges (mind the graphic representing the linear superposition because actually, cooling will open the crack, but heating will result in crack closure with the faces interpenetrating each other because no contact is modelled. The result is still of value because it can be added to any other linear problem from other loads to obtain COA and SIF)

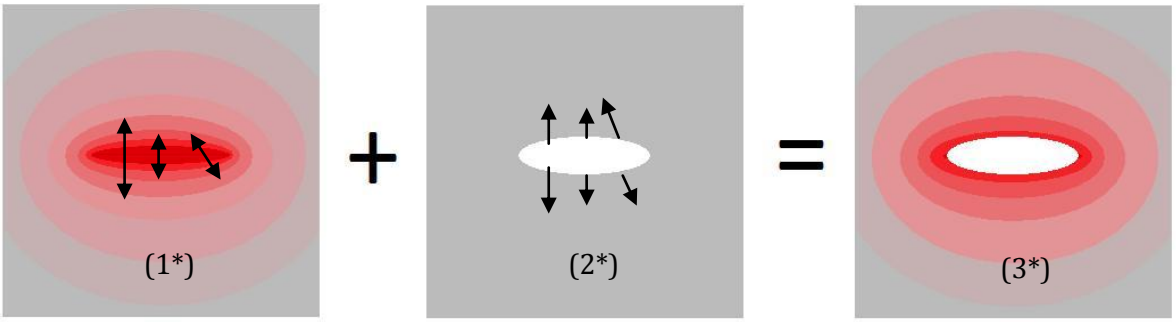

3.4-4 Principle of superposition for a thermo-mechanical including a crack

Also by linearity, the COA and SIF of the thermo-mechanical problem in the cracked plate (3*) can be obtained by taking the ones obtained in the auxiliary problem (2*) (since problem (1*) is in an uncracked plate, COA and SIF equal zero)

For a single source of heat of coordinates (*a,b*) in a continuous infinite plate (1*), the following formula applies for the stress along the y-axis in plane stress [10]

$$\sigma_{yy}(x,y)=\frac{\alpha E}{2\pi r^2}\left(\left[(b-y)^2-(a-x)^2\right]\left[\frac{K_1(\chi r)}{\chi r}-\frac{1}{\chi^2 r^2}\right]-(a-x)^2 K_0(\chi r)\right) \quad (3.44)$$

where K_1 is a first order modified Bessel function of second kind.

Thus the following stands for pressures on the crack rectilinear edges of problem (2*)

$$\sigma_d^0(r)=\sigma_d(x,0)|_a=-\sigma_{yy}(x,0)|_a=\frac{\alpha E}{2\pi}\left(\frac{K_1(\chi r)}{\chi r}-\frac{1}{\chi^2 r^2}+K_0(\chi r)\right) \quad (3.45)$$

where $r=x-a$

And the SIF can be easily computed using the following formula for a rectilinear crack of length 2l combined with the pressure stresses of a heat source

$$k_I(\pm l,a)=\frac{1}{\pi\sqrt{2l}}\int_{-l}^{l}\sqrt{\frac{l\mp x}{l\pm x}}\sigma_d^0(x-a)dx \quad (3.46)$$

The stress intensity factor in Mode I for problem (2*) or (3*) is obtained integrating the product of the elementary stress intensity factors for single sources, as follows

$$K_I(\pm l)=\int_{-l}^{l} p(a)k_I(\pm l,a)da \quad (3.47)$$

where $p(a)$ is the density of heat source found in (3.42) i.e 2q/k

so that combining equations (3.45), (3.46) and (3.47), the crack opening area is obtained for an infinite plate containing a rectilinear crack whose edge are subjected to a uniform heat flux

$$A(l)=\frac{2q\alpha}{\sqrt{2}\pi^{3/2}k\chi^4}\int_0^{\varepsilon}\varepsilon'\left(\int_{-\varepsilon'}^{\varepsilon'}\int_{-\varepsilon'}^{\varepsilon'}\sqrt{\frac{l-x}{l+x}}\left[\frac{K_1(x'-a')}{x'-a'}-\frac{1}{(x'-a')^2}+K_0(x'-a')\right]dx'da'\right)d\varepsilon' \quad (3.48)$$

where $\varepsilon=\chi l$

In the paper [10], the modified Bessel functions $K_0(\varepsilon)$ and $K_1(\varepsilon)$ are developed in series of ε up to the sixth order to compute the integrals when this parameter is of low value, i.e when the characteristic decaying distance of the temperature is big with respect to the crack length. The mode I stress intensity factor computed for the case of the crack subjected to a uniform flux is (the others are zero)

$$K_I(l)=\frac{\alpha Eql^{3/2}}{\sqrt{2}\pi k}\left[H_{30}^{+}+\frac{5}{16}\varepsilon^2H_1^{-}+\frac{21}{512}\varepsilon^4\left(H_{22}^{-}-\frac{11}{1260}\right)\right] \quad (3.49)$$

where $H_m^{\pm}=\ln\frac{\varepsilon}{4}+\gamma\pm\frac{m}{60}$

In the present work, this expression has been used to compute the related COA using (2.10) in section 2.1.1.2

$$A(l)=\frac{2\sqrt{2}\alpha ql^3}{3\sqrt{\pi}k}\left[H_{10}^{+}+\frac{3}{16}\varepsilon^2H_{13}^{-}+\frac{9}{512}\varepsilon^4\left(H_0-\frac{1}{7}-\frac{11}{1260}\right)\right] \quad (3.50)$$

These expressions are singular as ε goes to zero. Though correct, this is non-physical but not surprising because actually ε going to zero would mean that an infinite plate is totally insulated except on a surface with imposed flux, so that no equilibrium can be reach, and the thermal energy in the plate tends to be infinite. This wouldn't have been the case with an imposed temperature which bounds the local thermal energy.

3.4.4.2 Numerical model

The case was simulated numerically with Code_Aster. For this purpose a quarter of a thin plate in 3D has been modelled using the symmetries. In order to be close to the case of an infinite plate, dimensions of plate a lot bigger than the characteristic temperature decay length $1/\chi$ have been chosen. This length itself has to be big as compared to the crack length for the previous approximation to be valid. It is necessary to be careful with this choice because the characteristic decay length and shape of strain on one hand and displacement on the other hand are not known. This can alter the relevance of such theoretical solutions for a number of cases in real engineering situations where a crack is never truly remote from geometrical or thermal perturbation. For the case of a pipe, the curvature and the topology make it very different from the case of an infinite plate. It gives us an idea of how this kind of problem can be addressed, and could be the beginning of the development of models more

adapted to situations involving heated crack faces. This could lead to engineering corrections to COA in the presence of very high temperature fluids.

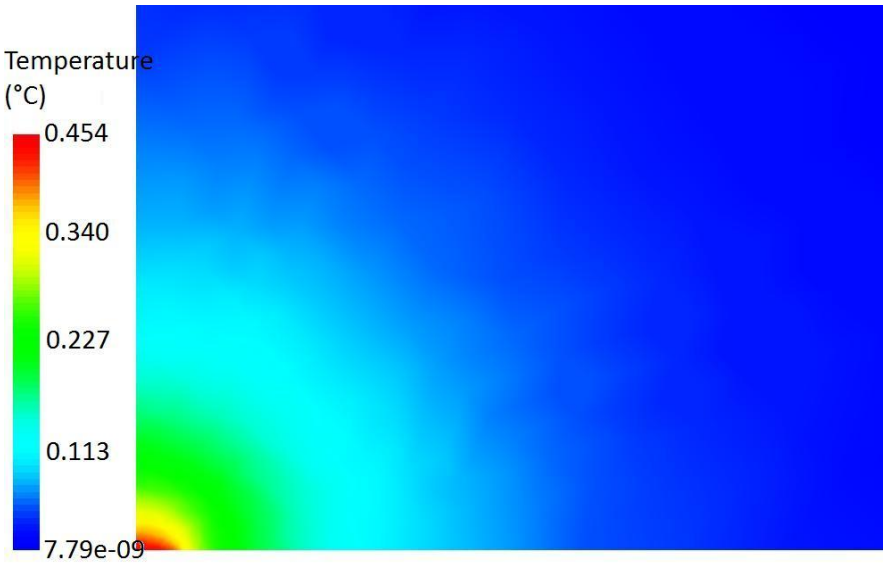

3.4-5 Temperature field in a plate containing a crack subjected to uniform heat flux

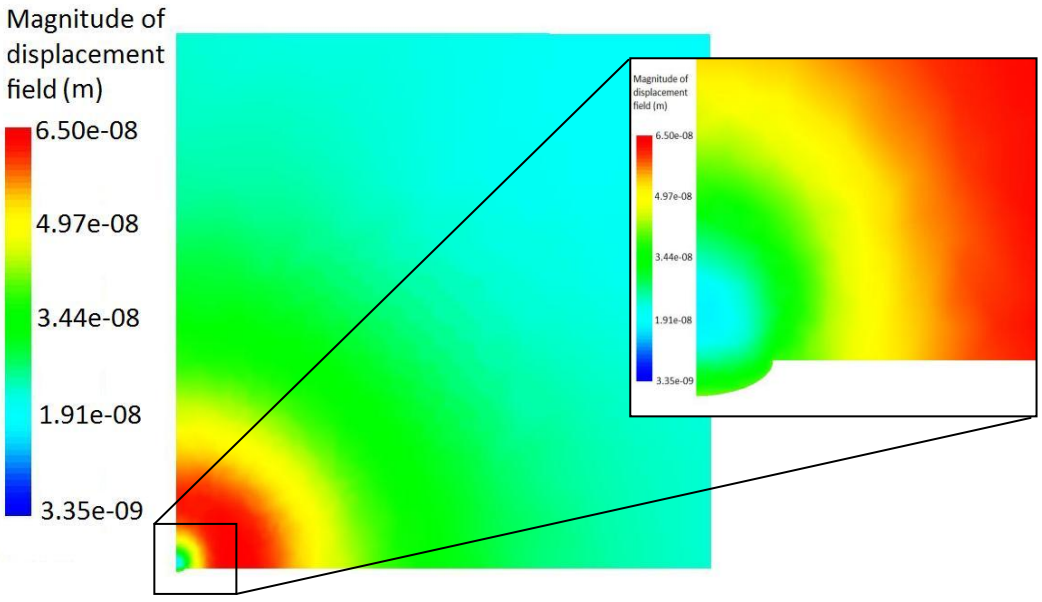

3.4-6 Deformed shape and displacement field magnitude for a heated crack in infinite plate

Note that on the figures and the related following results the opening area is negative. Of course, these results are valuable in a realistic manner only if this crack closure is compensated by crack opening forces. Otherwise, modelling of contact must be used.

Figures 3.4-5 and 3.4-6 respectively show the temperature and magnitude of displacement field in the plate for a configuration in which ε is set to 0,1. On the first figure, it can be

observed that the temperature is radially decaying from the crack to its value at infinity, set to nil, and so is consequently the thermal strain. The second figure is more complicated to interpret. The magnitude of displacement first increases with radial distance to the crack, then reaches a maximum before decaying to zero at infinity. This is because the most thermally stressed region is under compression, generating a negative crack opening and circumferential extension in the surrounding zone (like in an inflated balloon). This zone in extension (red zone on the picture) ensures the compatibility of displacement field around the compressive zone. Farther from the crack, the thermal loads are equilibrated so that the displacement field decays to zero at infinity.

For the theoretical formulae and for the numerical analysis, results are represented as functions of ε. The opening area is represented by the non dimensional normalized COA

$$A^*(l) = \frac{3\sqrt{\pi}k}{2\sqrt{2}\alpha q l^3} A(l) \tag{3.51}$$

Results of the comparison are shown in figure 3.4-7. Observe that the same shape is attained, giving credit to the theoretical model established in this section. Unfortunately, the values are quantitatively different, and the reason for that hasn't been clearly identified. It is possible that the numerical model used does not correspond to the mathematical model: the finite elements model is three-dimensional, so that there might be a slight temperature gradient in the thickness, fading remotely to zero, that might create an additional contribution to the COA and SIF. Another reason is probably that the effect being singular with ε, it makes the approximation rather sensitive to discretisation as the temperature is singular on the crack tip.

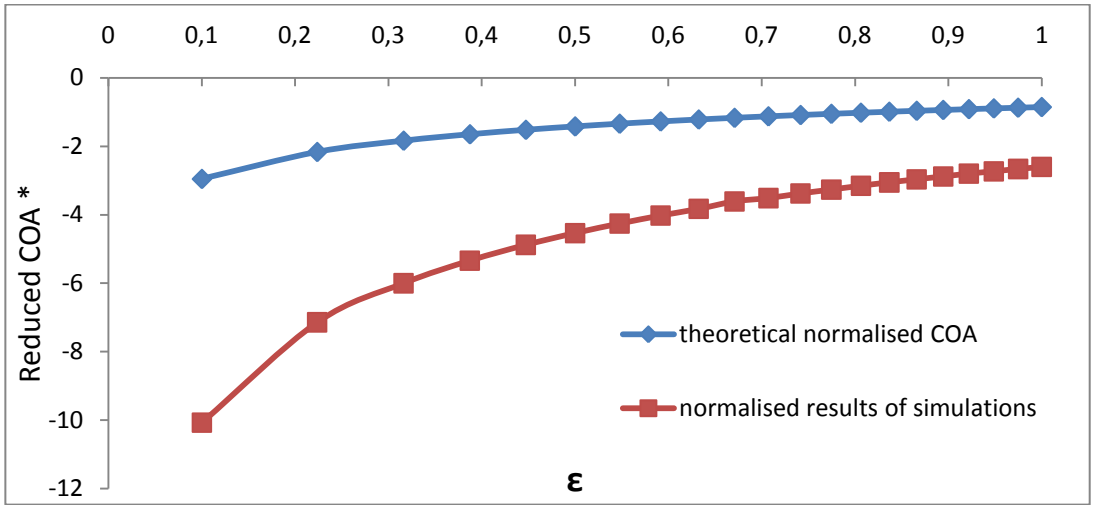

3.4-7 Comparison of normalised COA for a heated crack

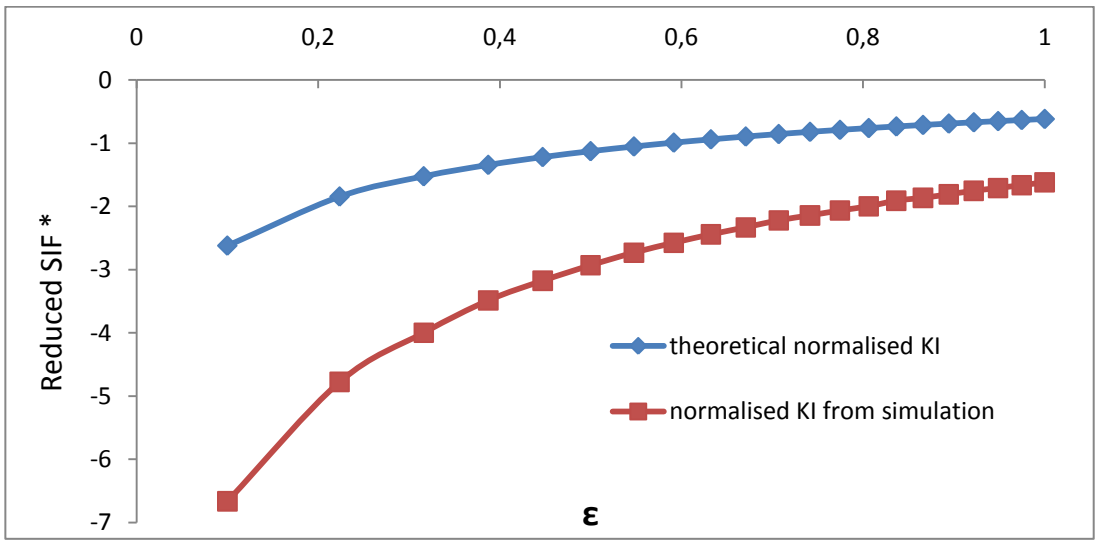

3.4-8 Comparison of normalised SIF for a heated crack

4 Influence of a specific geometrical feature on COA and SIF

In the scope of the present report, an additional study has been performed whose goal was to assess an example of the effect a specific geometrical feature can have on COA and SIF. Similar studies have been performed by Serco in previous papers [16] and [17]. Here the choice has been made to study the effect of a smooth change of thickness in a pipe at the location of a circumferential crack. Such a configuration is very commonly found in the nuclear industry, and in general for nozzles implanted in pressure vessels reinforced at the level of their basis. For example the most loaded kinds of nozzle in the nuclear industry are the inlet and outlet nozzles of a reactor pressure vessel.

4.1 Model geometry and properties

The presented geometry can be found in the nozzle of a Power Water Reactor as shown in the following figure 4.1-**1**

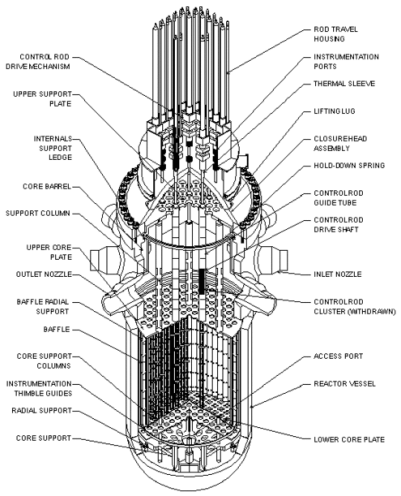

4.1-1 Reinforced nozzles implanted pressure vessel of a nuclear power plant

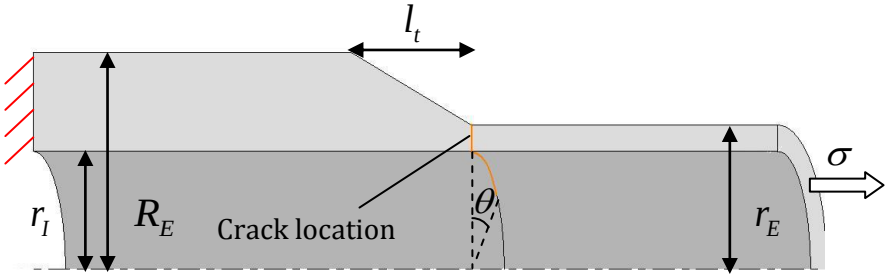

4.1-2 Geometrical configuration of the pipe with thickness transition

The geometry chosen (see figure 4.1-2) is a pipe of constant interior radius R_I. The exterior radius was variable. First it is constant with value r_E, and then at the circumferential crack location, the pipe thickens linearly up to another constant radius R_E.

The study was performed in linear elasticity only with a Young's modulus of 200GPa and Poisson's coefficient of 0,3.

4.2 Mesh

By symmetry, only a half pipe was modelled, but the dissymmetry of the structure with respect to the crack doesn't allow representing only one of its faces. In this case, a crack is required to be inserted in the mesh. In order to do that, a script has been programmed to build the pipe and a refined area on the crack front automatically from given dimensions. Then two solutions have been tried to create a crack in the pipe, giving identical results

- Two distinct parts of mesh are created separately and fused together by fusing any coincident nodes and elements, except on the crack faces.
- Only one mesh is created, and a crack is inserted by doubling the nodes and elements in all the groups of elements.

19840 linear 3D elements (HEX8) with degrees of freedom DX, DY, DZ have been used for this study.

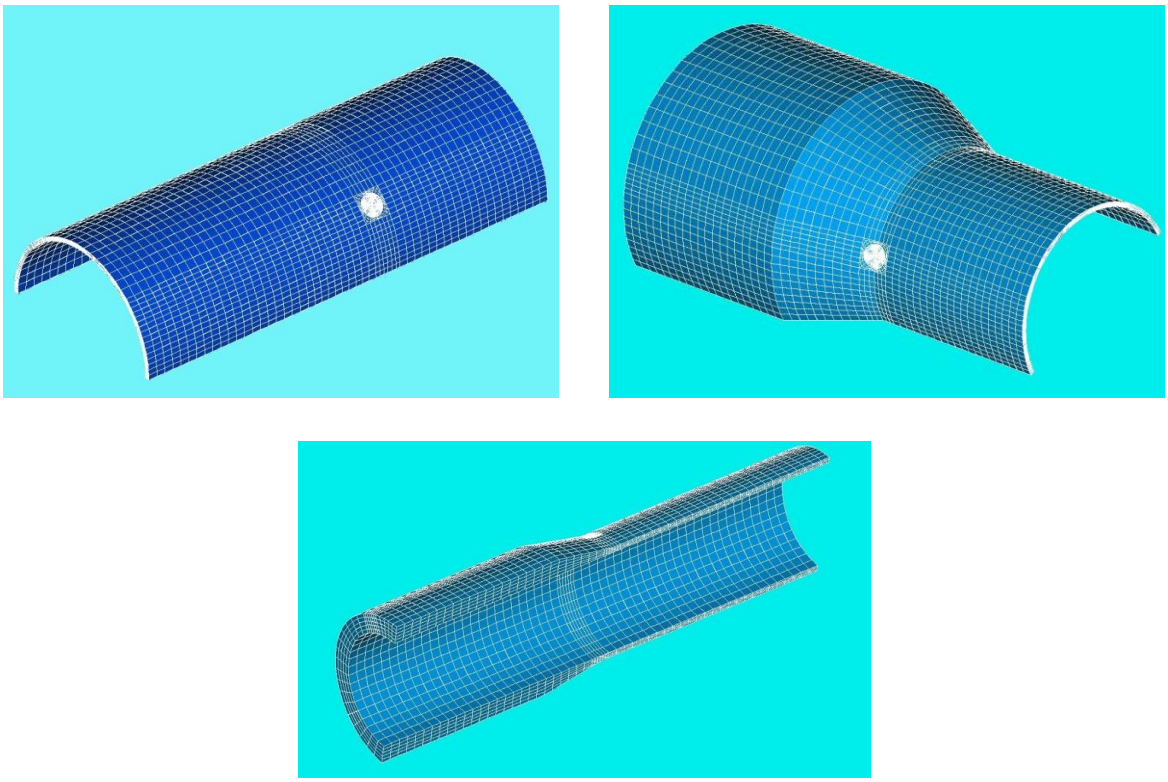

4.2-1 Different examples of meshes of pipes with thickness transition and refined crack

4.3 Loading and fracture mechanics post-processing

To investigate the effect of the thickness transition, the pipe was subjected to an axial tensile stress by applying a uniform negative pressure on the section of the pipe of small thickness. In linear elasticity, an arbitrarily chosen remote stress can be applied to determine the solution for any stress, so that the results have been normalised by the values for the case of the pipe with constant radius over its whole length.

For a plate of curvature zero and of constant thickness, the COA and SIF do not depend on the thickness, so that the most natural parameter to characterise the transition is likely to be the relative slope i.e. the slope of the radius in function of axial coordinate divided by the thickness of the part in which the crack lies. Therefore, COA and SIF have been computed for several geometries as a function of the relative slope parameter

$$S_r = \frac{1}{r_E - r_I}\frac{\partial r}{\partial x} = \frac{R_E - r_E}{\left(r_E - r_I\right) l_t} \tag{4.1}$$

Dependencies on the boundary conditions have been explored to ensure that the results were not too depending on the finite dimensions of the modelled structure. For this purpose, some samples of the results have been reproduced with a pipe length twice the size of the model used in the general case, with a high crack angle of 30°. The results would then differ from less than one percent.

Also, to ensure that the results were universal with regard to the relative slope, it has been checked whether the finite length of the part with increasing radius would modify them. It is expected that the influence can be made independent over a range of length scales, because the modification of COA and SIF will be low when the relative slope is low, whereas the stress field perturbed by the crack will be rapidly dampened with the increasing thickness when it is big. By doubling the length of the transition for a relative slope of$10m^{-1}$, a ratio R/t of 10 and a crack angle of 30°, the results in energy release rate were equal by less than 3%.

The crack opening areas at the bottom of the crack and at its outer surface have been obtained by calculating the differences of the integral of axial displacement (crack opening direction) respectively on the inner and outer edges of the crack faces. Then the crack opening area has been taken as the mean between these two values.

4.4 Results

The plate on one side of the crack being thicker, it is easy to think that it will be less subjected to deformation, and that as a consequence the crack opening area will be of lower value. With the results obtained by the elastic simulations, this is possible to quantify the intensity of this shielding effect. They are likely to tend towards the case of an infinite slope, which is in fact

the pipe embedded in a semi-space material of same mechanical properties. As a large mass is unlikely to be deformed a significantly, the limit COA and SIF should be a bit above half respectively the COA and SIF for a straight pipe. On figure 4.4-1, the SIF has been normalised by the one obtained for a straight pipe, and plotted against the relative slope. The shielding factor for SIF rate is defined by $SIF/SIF_{straight}$

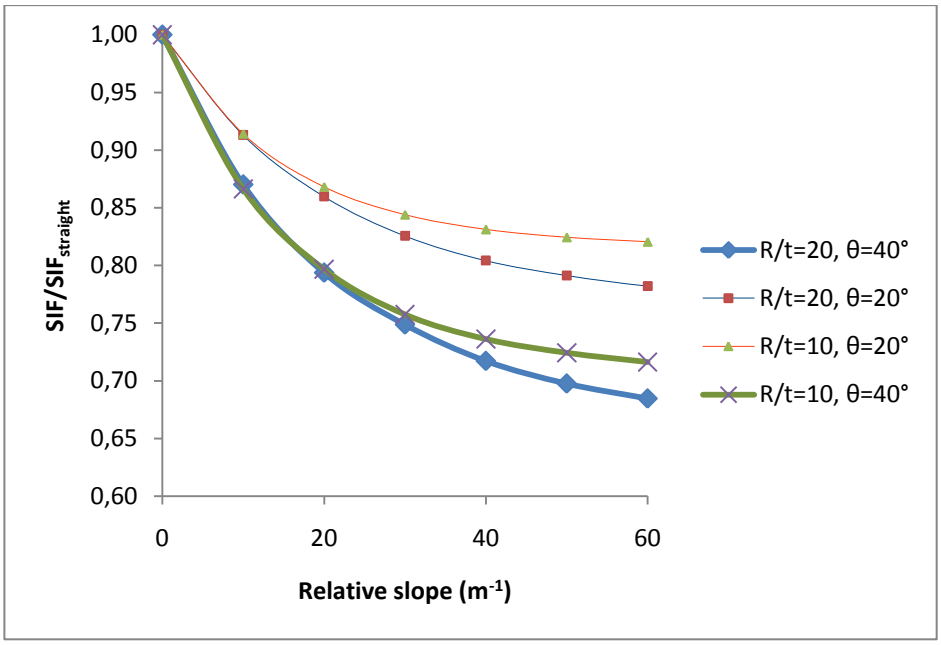

4.4-1 Shielding factor versus relative slope for different geometries

This evolution can be observed on figure 4.4-1. It represents the SIF as a function of the relative slope for various ratio R/t and crack angles. The shielding effect increases with the relative slope and its influence is particularly dependant on this parameter close to the case of the straight pipe, that is why these cases should be addressed with great care.

Note also that for a same crack angle the tangent to the curve at coordinate zero seems to be the same, so that for small relative slope, the shielding doesn't depend on the ratio radius on thickness anymore. For higher values of the relative slope though, a slightly higher shielding effect is observed for thinner pipes i.e. high ratio.

Exactly the same qualitative conclusions can be drawn for the values of normalised COA i.e the shielding factor for COA, $COA/COA_{straight}$ in figure 4.4-2

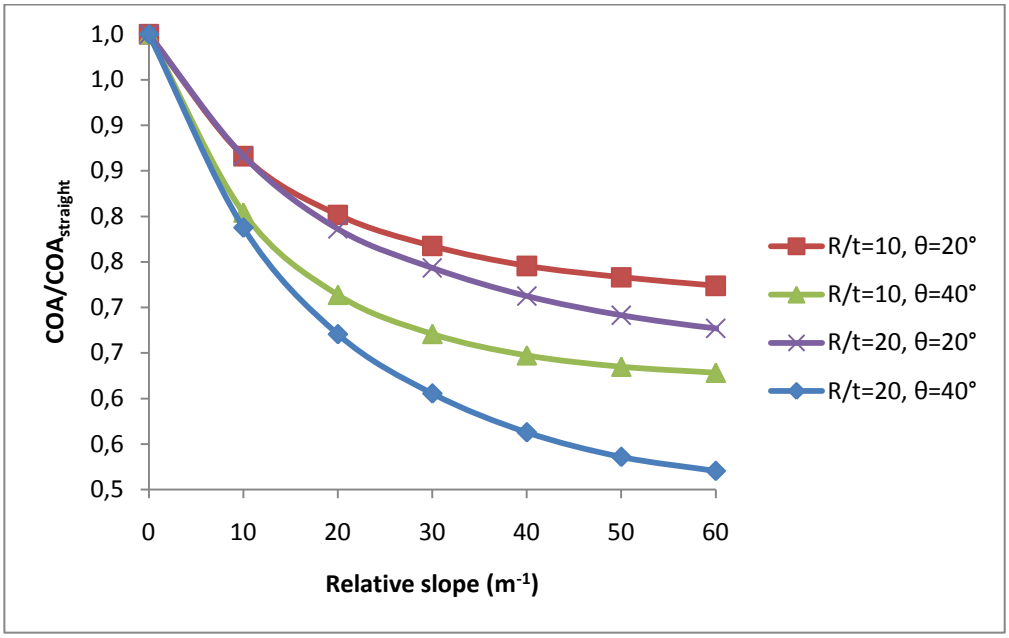

4.4-2 Shielding factor for COA versus relative slope for different geometries

In order to have a better understanding of the effect of thickness transition with regard to crack angle, the bulging factor and the shielding factor for energy release rate have also been plotted against the crack angle for a relative slope of 20 m^{-1} for R/t=10, using the following expressions

$$F_t = \frac{K_I}{\sigma\sqrt{R\theta}} \tag{4.2}$$

$$S_{SIF} = \frac{K_I}{K_{I\_straight}} \tag{4.3}$$

where F_t is the bulging factor as defined in section 2.1, S_{SIF} is the shielding factor for SIF, and $K_{I\_straight}$ the SIF that would be obtained on a straight pipe having the minor thickness all along and subjected to the same load.

The results are shown figure 4.4-3 and 4.4-**4** respectively. The results for bulging factor for a straight pipe are compared to the simple solution from Tada and Paris [13] in order to control the agreement with previous solutions. It can be observed that the bulging is more than compensated by the thickness transition for small angles. The shielding factor for SIF was also plotted against the crack angle on figure 4.4-**4**. This time it can be clearly seen that it decreases with the crack angle.

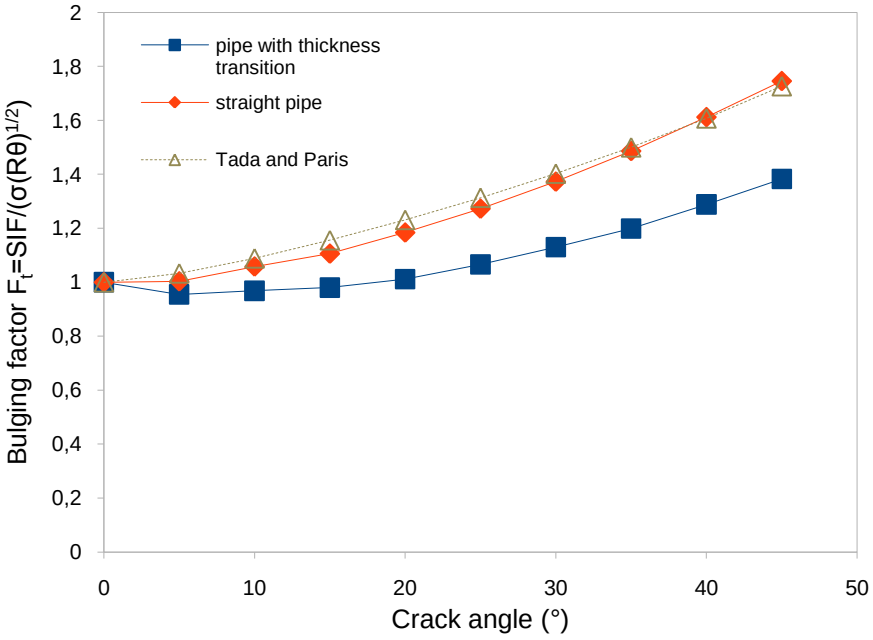

4.4-3 Bulging factor versus crack angle with and without thickness transition

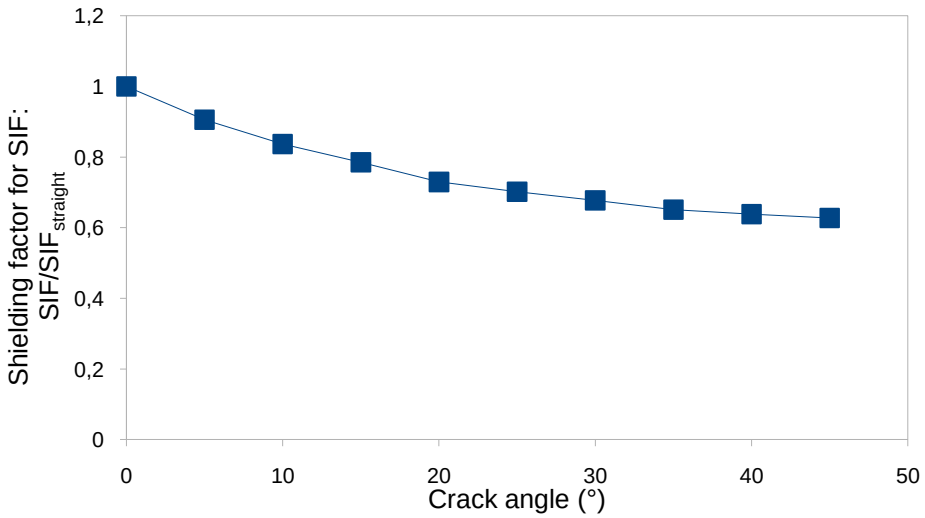

4.4-4 Shielding factor versus crack angle

4.5 Conclusion

The results show that great care must be taken when assessing a crack lying at the location of a change in thickness, because it can have a significant influence; the latter is particularly high for cracks whose length is comparable to the shell curvature radius. As far as leak before break is concerned, the comparison with the results for a straight pipe shows that the values of COA and SIF are attenuated by the shielding due to the change in thickness. Therefore, consideration of a straight pipe when dimensioning piping systems represents a conservative assumption for damage accumulation in fast fracture. But on the contrary, the calculations involved would incorrectly overpredict the flow rate to be above the detection threshold.

5 General conclusion

A general overview of the philosophy of LBB analysis has been made and techniques of evaluation of COA, SIF and leak rates have been presented, giving a general idea of what main concerns are in addressing LBB cases.

Then the need to couple the fluid leaking through a crack and the structure has been investigated using previous developments by EDF enhanced for the purpose of fracture mechanics. The study points out a significant particular example that the fluid has an influence on COA, SIF and leak rates. Taking into account the pressure is relatively straightforward, as it acts just as a remote stress and its value is bounded by the internal pressure. As for the temperature generated by the heat exchange on the crack faces, it is much more difficult to evaluate its influence on LBB analysis, on one hand because the stress and temperature fields become quite complex in such geometries, and on the other hand because the heat flux is not known and in turn very dependent on the displacement and temperature fields in the crack. So where a significant influence of temperature is suspected, it is recommended to use finite element analysis with coupling, such as made possible by Code_Aster and Ecrevisse, especially as a potential underestimation of crack opening area is been suspected. Though one method to determinate crack opening areas for cracks subjected to heat flux has been presented, its range of application is rather limited and could not be used for instance to address engineering problems involving pipes.

A particular case of dependence to geometry of pipes has been presented in the present report, and has shown that great care must be taken in using formulae for a straight pipe when assessing cracks in the vicinity of changes in thickness, thus needing to use adequate margins.

As a conclusion, it is evident that evaluation of COA, SIF and leak rates for the purpose of LBB analysis is not a simple engineering problem, and great care and engineering judgment must be employed for a real component where the influence of the fluid, the geometry and the material properties are stained with great uncertainty.

6 Recommendations for Further Work

From a theoretical point of view, the influence of a coupling with a fluid has to be investigated in depth, because this is a very complex problem. In the model of the heated crack, it could be of interest to apply mixed temperature boundary conditions of Newton type with the same kind of method presented here. Interesting also is the development of solutions and bulging factors for heated cracks in pipes and pressures vessels. These would probably be the simplest model applicable to real engineering problems. A particular influence of the temperature inside the crack on creep can be suspected, but this should be readily addressed with recommendations of R6 and above all of R5 which presents high temperature operations.

As far as numerical simulation is concerned, one could incorporate into the coupling scheme the soon-to-be scripts of EDF made to give as an input for Ecrevisse the full geometry of the modelled crack, instead of a mere crack opening displacement. A coupling with CFD code Saturn from EDF is currently being studied by a PhD student at Manchester University, but Ecrevisse is likely to be more adapted to a leak through a crack.

Also, other simple cases of geometries should be addressed with finite element analysis, in order to ascertain the conservatism in every case of standard formulae for pipes, and if not recommend adequate margins, both in bending and tensile stress, and also with elastic-plastic simulations.

7 References

1. Abaqus Theory Manual 6.7 PR6.
2. **EDF R&D.** Documentation Code_Aster V10 (www.code-aster.org). consulted July 2009.
3. **EDF R&D (2006).** Simulation d'écoulement air/eau/vapeur à travers une fissure : logiciel ECREVISSE version 3.1 Manuel utilisateur.
4. **Forman R. G., Hickman J. C., Shivakumar V. (1985).** Stress intensity factors for circumferential through cracks in hollow cylinders subjected to combined tension and bending loads. Eng. Frac. Mech. 21, 563-571
5. **Ghosh B., Bandyopadhyay S. K., Lele H. G., Ghosh A. K. (2009).** Estimation of crack opening area for leak before break analysis of nuclear reactor system. Nucl. Eng. Des. 239, 327-337
6. **Hervouet C. (2005), .** Simulation d'écoulement air/eau/vapeur à travers une fissure : logiciel ECREVISSE version 3.0 Note de principe. HI-86/04/005/A.
7. **International Atomic Energy Agency, Vienna (1993).** Applicability of the leak before break concept. TECDOC-710.
8. **Kaster et al., (1981).** Critical crack sizes in ductile piping,. Int. J. PVP 9,197-219.
9. **Kim Y-J, Huh N-S, Kim Y-J, Yang J-S (2003).** Engineering Leak-Before-Break analyses of pressurized piping: Part I Crack opening Displacement . JSME Int. J. A 47, 4, 525-536.
10. **Kit G. S., Nechaev Y. K., Poberezhnyi O. V. (1977).** Determination of the stress intensity factors of a plate subjected to heat transfer. Trans. Prildadnaya Mekhanika 13, 4, 66-71
11. **Klecker R., Brust F. W., Wilkowski G. (1986).** NRC Leak-Before-Break (LBB.NRC) analysis method for circumferentially through-wall cracked pipes under axial plus bending Loads, NUREG/CR-4572
12. **Lacire M. H., Chapulliot S., Marie S. (1999).** Stress intensity factors of through-wall cracks in plates and tubes with circumferential cracks. ASME PVP 388, 13-21.
13. **Paris P. C., Tada H. (1983).** The application of fracture proof design methodology using tearing instability theory to nuclear piping postulating circumferential throughwall crack, NUREG/CR-3464

14. R6: Assessment of the Integrity of Structures Containing Defects, British Energy Generation Limited, Revision 4 (2001).

15. **Streitenberger P., Knott J. F. (1996).** The calculation of crack opening area and crack opening volume from stress intensity factors. Int. J. Frac. 76, 49-54

16. **Sharples J. K., Hooton D. G., Charles R., Dodia H., Budden P. J. (2008).** Recent developments to improve crack opening areas for R6 leak-before-break procedures. ASME PVP 2008, PVP2008-61064.

17. **Sharples J. K., Charles R., Madew C. J., Budden P. J. (2009).** Crack opening area solutions for through-wall cracks in the vicinity of welded attachments. ASME PVP 2009, PVP2009-77087.

18. **Takahashi Y. (2002).** Evaluation of leak-before-break assessment methodology for pipes with a circumferential through-wall crack. Part III: estimation of crack opening area. Int. J. PVP 79, 525-536.

19. **Takahashi Y. (2003).** Comprehensive Structural Integrity. Elsevier, 7, 7.10 Leak-Before-Break.

20. **Wüthrich C. (1983).** Crack opening areas in pressure vessels and pipes. Eng. Frac. Mech. 18, 5, 1049-1057.

21. **Zahoor A. (1985).** Closed form expression for fracture mechanics analysis of cracked pipes. Trans. ASME J. Pres. Ves. Technol. 107, 203-205.